

Response to reviewers

We are very grateful for the constructive feedbacks provided by the 3 reviewers that helped us to significantly improve our manuscript. Below, we present a point-by-point response to all the individual comments raised.

We have carefully considered and addressed all comments and suggestions of the reviewers. This led to additional text and revised Figures in the revised version according to reviewer suggestions. We also added a new Appendix B: “Application of our calibration to other past periods” in the revised version, containing the additional tests we conducted during the review process for the MH and LIG time periods which allow us to contextualize our results for different climate periods. The Code and Data Availability section has been updated to indicate that the Python code for the Bayesian calibration models and the new dataset are freely available at the following repository: https://github.com/nicrie/density_uncertainty.

In our response to the reviewers' comments, we present some results of data-model comparison from the paper of Barathieu et al., that will be submitted very soon, to show that the models used in our study (MPI and iLOVECLIM) exhibit significant (p-value <0.05) and strong correlation ($R^2>0.5$) with our reconstructed densities for the PI and LGM.

Reviewer comments are shown in **red color**, with our responses in black.

Changes in the manuscript version (marked-up manuscript version) are in red color.

Sincerely,

Thibaut Caley on behalf of all co-authors

35 **Response to Reviewer 1**

36 Caley et al. calibrate planktic $\delta^{18}\text{O}$ from core tops to surface density and assess the
37 uncertainty via Bayesian modelling. The authors test the calibration with the results of
38 isotope enabled models and apply the method to foraminiferal $\delta^{18}\text{O}$ values from the Last
39 Glacial Maximum and the late Holocene. The attempt to translate $\delta^{18}\text{O}$ directly into density
40 is certainly worthwhile since we have probably an order of magnitude more $\delta^{18}\text{O}$ data
41 available compared to combined $\delta^{18}\text{O}$ /temperature reconstructions. However, the paper has
42 methodological and transparency issues that need to be addressed.

43 **1. Representation of mean ocean density.** There are surface density changes related to
44 local/regional SST and SSS changes and mean ocean density changes related to ocean
45 volume. Part of the local/regional density changes will be related to mean ocean salinity due
46 to volume changes with sea level. For example, Duplessy et al. (1991) estimated that the
47 smaller LGM ocean volume led to ~ 1 psu higher salinity (and hence a significantly higher
48 global ocean LGM density). In principle, foraminiferal $\delta^{18}\text{O}$ contains information on sea level
49 via the ice effect (albeit with a higher slope as usual evaporation -precipitation changes). The
50 $\delta^{18}\text{O}$ ice effect, however, is removed before the LGM density reconstruction. Can the LGM
51 reconstructions really reflect absolute density or have the authors rather reconstructed the
52 density changes due to local/regional changes in SST and SSS? Perhaps I am missing
53 something here, but in my view the mean ocean density changes corresponding to mean
54 ocean salinity changes due to ice/ocean volume changes have to be added to the LGM
55 values since the used foraminiferal isotope data do not contain this information and the
56 method does not account for it. This point requires further clarification.

57 We thank the reviewer for this thoughtful comment and we agree with the reviewer that
58 this point requires further clarification in our paper. What we reconstructed are indeed the
59 density changes due to the hydrographic changes in SST and SSS (the local/regional SST and
60 SSS changes mentioned by the reviewer). To determine mean ocean density changes related
61 to ocean volume we used model simulations results (ECHAM/MPI-OM and iLOVECLIM) and
62 added or removed 1 psu salinity in global salinity outputs. Note that adding or removing 1
63 psu of salinity at LGM in climate model simulations have only small effects on ocean
64 dynamic. Indeed, the effect is due to the small non-linearity in the sea-ice freezing, hence
65 generating small differences in regions of sea ice and deep water formation. We have tested
66 it in new simulations performed with the iLOVECLIM model and found the dynamical effect
67 of that 1 psu in the regions we are analyzing to be very small (not shown). We also added or
68 removed 1 ‰ in the ocean $\delta^{18}\text{O}_{\text{sw}}$ reflecting the global mean ice-sheets contribution.

69

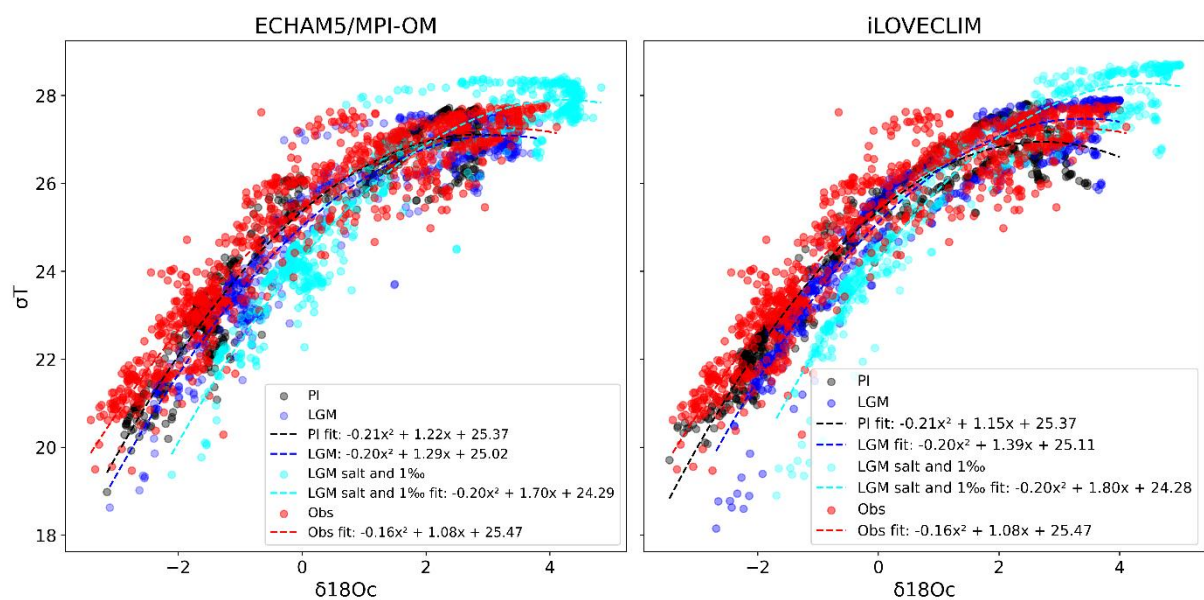
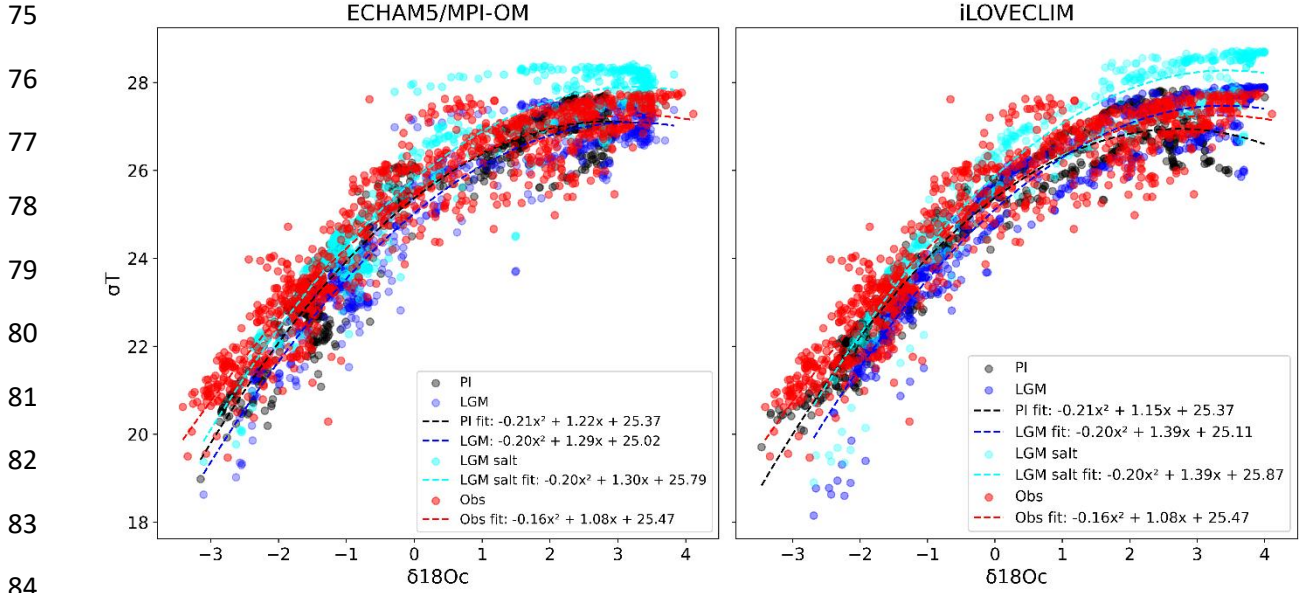
70

71

72

73

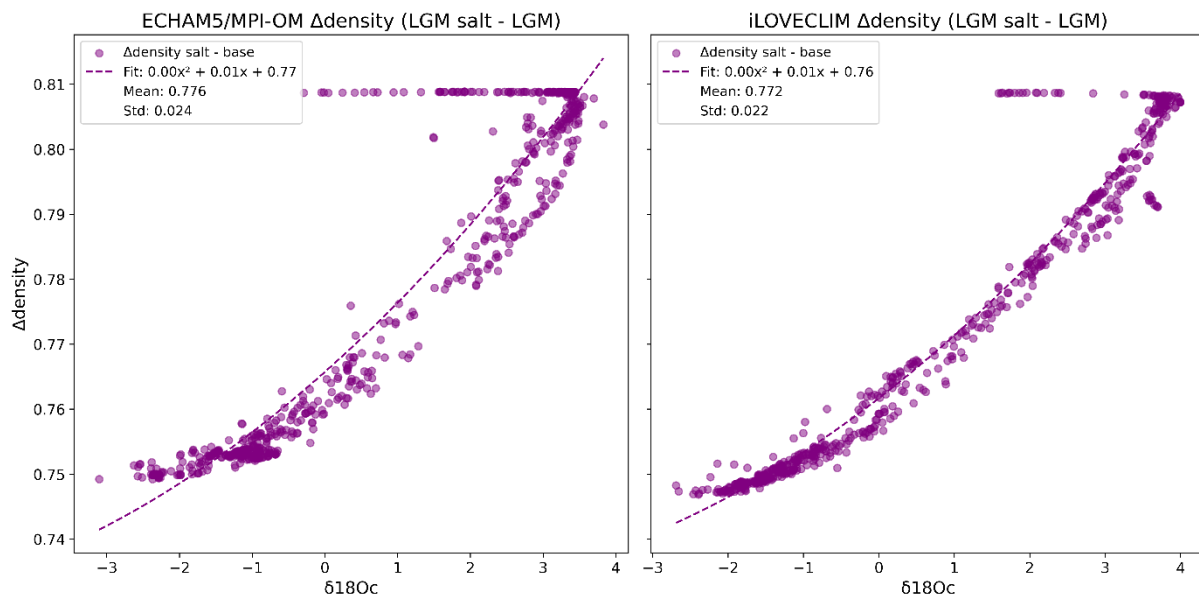
74



93 In Figure a1 we observe how a change in + 1 (cyan color) or - 1 (blue color) psu salinity in
 94 model simulations affect the surface density at the LGM and so the $\delta^{18}\text{Oc}$ -density relation. In
 95 Figure a2, the cyan colour data show the $\delta^{18}\text{Oc}$ -density relation at the LGM (with + 1 psu
 96 salinity and +1 ‰ $\delta^{18}\text{Osw}$) contrary to Figure a1 that only contain + 1 or - 1 psu salinity in

97 model simulations. The $\delta^{18}\text{O}_{\text{C}}$ -density relation at the LGM (with + 1 psu salinity and +1 ‰
98 $\delta^{18}\text{O}_{\text{sw}}$, cyan colour) can be used to estimate LGM density. To reconstruct absolute density
99 at the LGM with the observed relation (red color on Figures a1 and a2), we can remove the
100 $\delta^{18}\text{O}$ ice effect (1‰) but need to add mean ocean density changes corresponding to mean
101 ocean salinity changes due to ocean volume changes (Figure a1). If not added, we indeed
102 reconstruct the density changes due to hydrographic changes in SST and SSS (the
103 local/regional SST and SSS changes mentioned by the reviewer).

104 We calculated mean ocean density changes corresponding to mean ocean salinity changes
105 due to ocean volume changes by adding or removing +1 psu of salinity during the LGM in
106 model simulations (Figure b).



107
108 Figure b: surface ocean anomaly of density when +1 psu is added or removed during the
109 LGM at the location of our core top observations used in our calibration

110 Figure b shows the surface anomaly of density when +1 psu is added or removed during the
111 LGM at the location of our core top observations used in our calibration. Both model
112 simulations agree and yield a mean ocean salinity effect on density of 0.776 ($\sigma = 0.02$) for
113 ECHAM/MPI-OM and 0.772 ($\sigma = 0.02$) for iLOVECLIM.

114 We also performed a calculation to estimate this effect based on observation (reference
115 state based on present day observation and LGM state based on Tierney et al., 2020 for SST
116 and Duplessy et al., 1991 for SSS). To calculate uncertainties, we use a bootstrap simulation
117 approach (uncertainties of ± 0.1 g/kg for salinity and of ± 0.2 °C for temperature) to estimate
118 the isolated effect of increased salinity on surface seawater density under Last Glacial
119 Maximum (LGM) conditions (10,000 samples of temperature and salinity anomalies are
120 randomly drawn using a uniform distribution to reflect plausible variability).

121 Reference State Definition: Modern ocean conditions are used as a baseline, with surface
122 salinity of 34.7 g/kg and temperature of 13.85 °C.

123 Perturbation Parameters: A salinity anomaly of $+1 \text{ g/kg} \pm 0.1$ is applied (Duplessy et al.,
124 1991). A surface temperature anomaly of $-2.9 \text{ }^{\circ}\text{C} \pm 0.2$ simulates cooler LGM conditions
125 (Tierney et al., 2020).

126 Results of mean surface density anomaly corresponding to mean ocean salinity changes due
127 to ocean volume changes (LGM context): 0.772 kg/m^3 95% confidence interval: (0.698 to
128 0.845 kg/m^3 .

129 Results and uncertainties are in very good agreement with model simulations results (Figure
130 b).

131 **Therefore, depending what we want to reconstruct, absolute density or density changes
132 linked to hydrographic changes in SST and SSS (the local/regional SST and SSS changes
133 mentioned by the reviewer), we need or not need to have an additional correction. For
134 absolute density, an additional correction is necessary, estimated to be equal to 0.77.**

135 We therefore added a new section “Reconstruction of past ocean surface absolute density”
136 to the text before section “3.2 LGM annual surface density reconstruction” in which we
137 explain that around +0.77 needs to be added to obtain absolute surface density values.

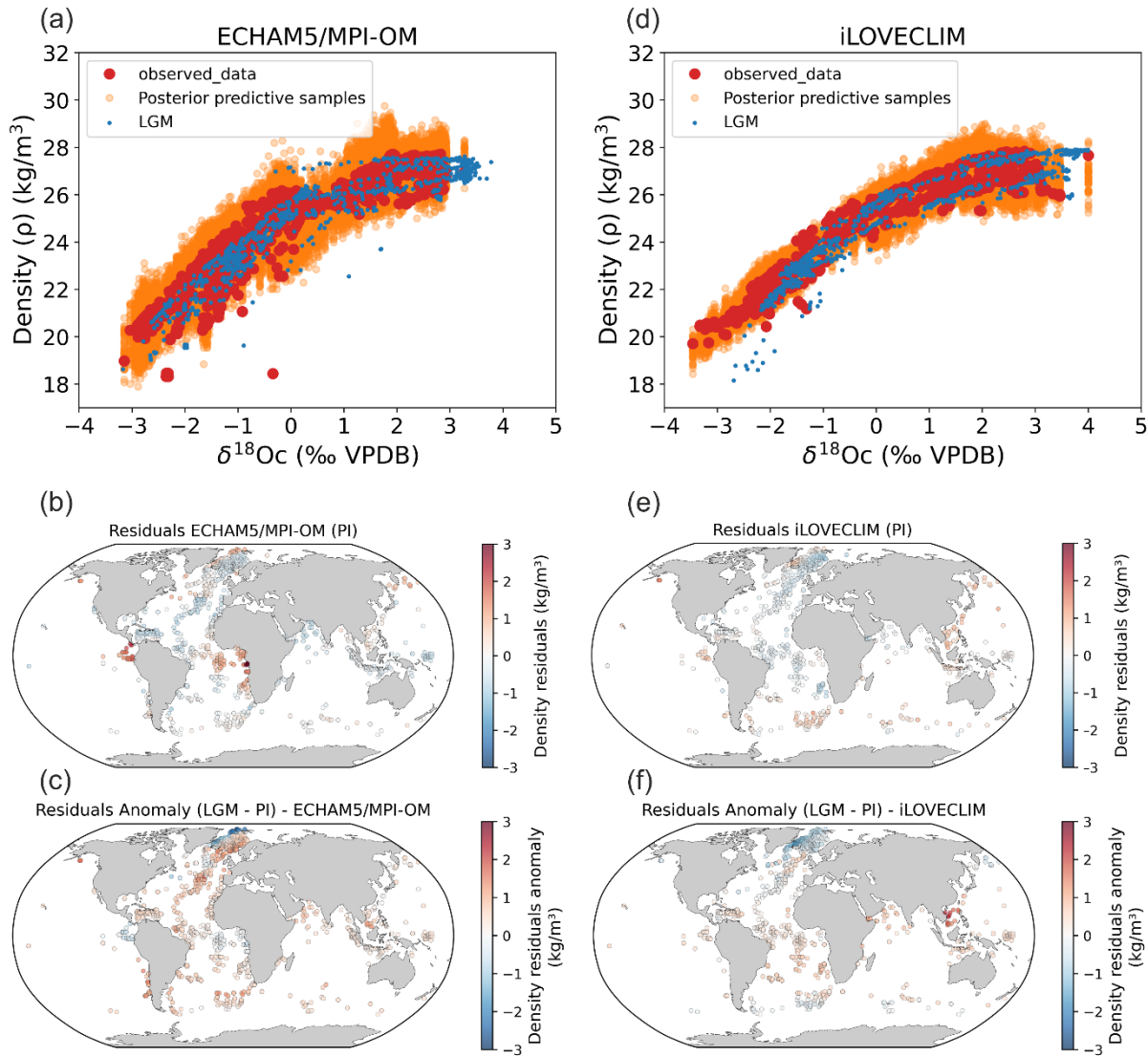
138 We added in lines 496-518: “3.2 Reconstruction of past ocean surface absolute density
139 To reconstruct past ocean surface absolute density based on foraminifera $\delta^{18}\text{O}_{\text{C}}$ values that
140 have been corrected from the $\delta^{18}\text{O}_{\text{sw}}$ ice effect, an additional correction is necessary.
141 Indeed, it is necessary to account for mean ocean density changes related to ocean volume
142 changes that affect mean ocean salinity. Without this additional correction, the ocean
143 density reconstructed corresponds to density changes linked to hydrographic changes in SST
144 and SSS.

145 To determine the mean ocean density change related to the change in ocean volume at LGM
146 we used model simulation results (ECHAM/MPI-OM and iLOVECLIM) and added or removed
147 1 psu salinity (Duplessy et al., 1991) in global salinity outputs. Note that adding 1 psu of
148 salinity at LGM in climate model simulations has only small effects on ocean dynamics.
149 Indeed, the effect is due to the small non-linearity in the sea-ice freezing, hence generating
150 small differences in regions of sea ice and deep water formation. We have tested it in new
151 simulations performed with the iLOVECLIM model and found the dynamical effect of a 1 psu
152 salinity change in the regions we are analyzing to be very small (not shown).

153 Both model simulations agree and yield a mean ocean salinity effect on density of 0.776 ($\sigma = 0.02$) for ECHAM/MPI-OM and 0.772 ($\sigma = 0.02$) for iLOVECLIM. We also performed a
154 calculation to estimate this effect based on observations (reference state based on present
155 day observations and LGM state based on Tierney et al., 2020 for SST and Duplessy et al.,
156 1991 for SSS) and found very consistent results (<https://doi.org/10.5194/egusphere-2025-2459-AC1>).

157 Therefore, the additional correction that is necessary to reconstruct past ocean absolute
158 density at the LGM is estimated to be equal to + 0.77.”

161 In part 3.2 we now propose the reconstruction of absolute density together with the density
 162 changes due to hydrographic changes in SST and SSS (the local/regional SST and SSS changes
 163 mentioned by the reviewer) for comparison and discussion (including a revised version of
 164 Figure 7). Figures 5 and 6 have been also revised to take into account mean ocean density
 165 changes related to ocean volume between iLOVECLIM and ECHAM/MPI-OM.

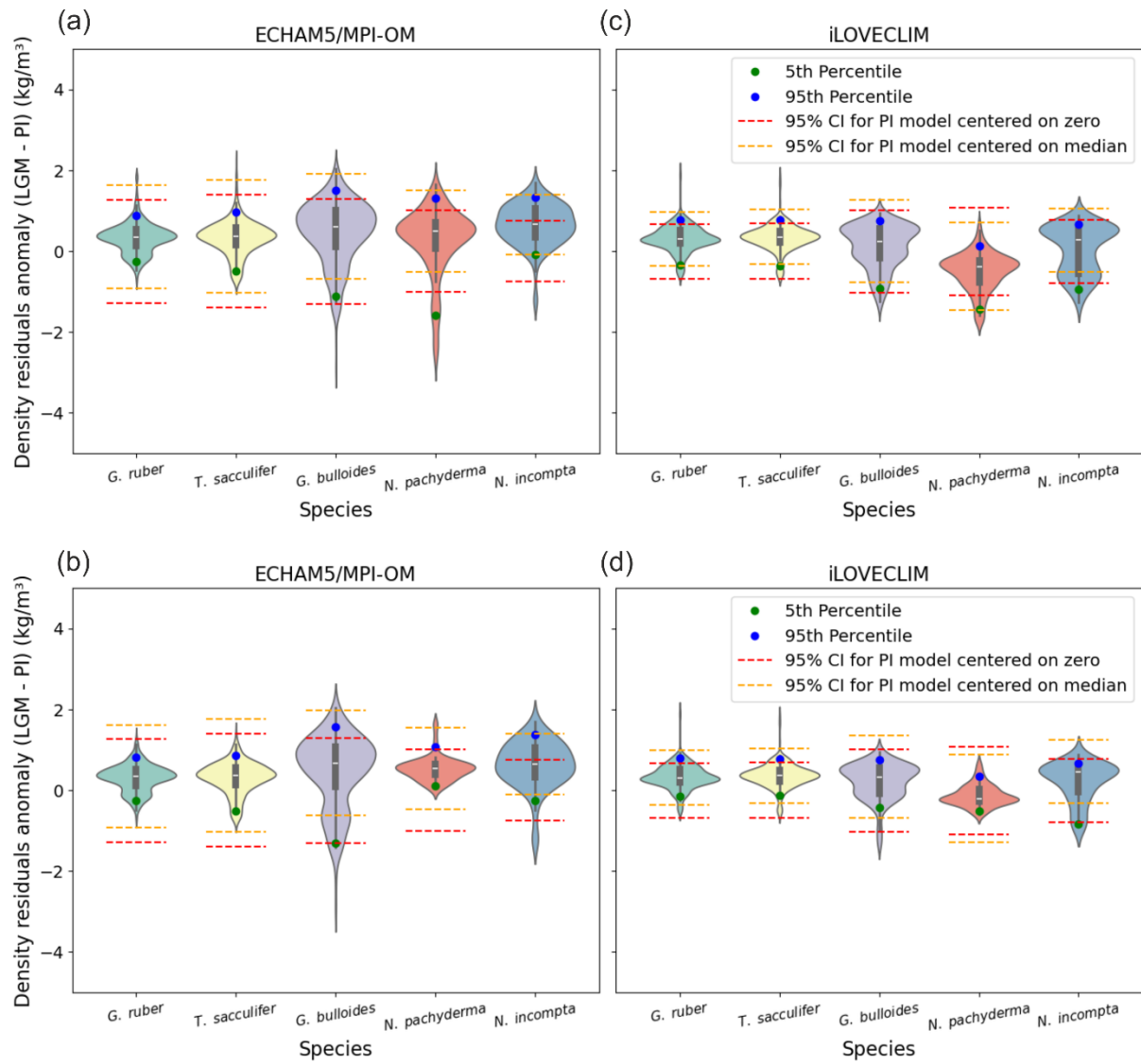


166
 167 Revised Figure 5: Stability of foraminifera $\delta^{18}\text{Oc}$ -density relations between PI and the LGM
 168 calculated with FAME and forced by global ECHAM5/MPI-OM (left panels, Werner et al.,
 169 2016) and iLOVECLIM (right panels, Caley et al., 2014) hydrographic data. (a) and (d) PI
 170 Bayesian regression models between foraminifera $\delta^{18}\text{Oc}$ and annual surface density. Data in
 171 the PI experiments have been selected at the same locations as observations (Fig. 1).
 172 Posterior predictive samples and the LGM $\delta^{18}\text{Oc}$ -density relation (LGM) are visible. (b) and
 173 (e) Density residuals (predicted - observed) for the PI experiments. (c) and (f) Density
 174 residuals anomaly between LGM and PI. Results for the Mediterranean Sea have been
 175 excluded because of its difficulty to be simulated and inconsistency between the two model
 176 simulations because of their different grid resolutions. Annual mean temperature and
 177 $\delta^{18}\text{O}_{\text{sw}}$ were used for the iLOVECLIM experiment whereas monthly temperature and
 178 $\delta^{18}\text{O}_{\text{sw}}$ were used for the ECHAM5/MPI-OM experiment.

179

180

181



182

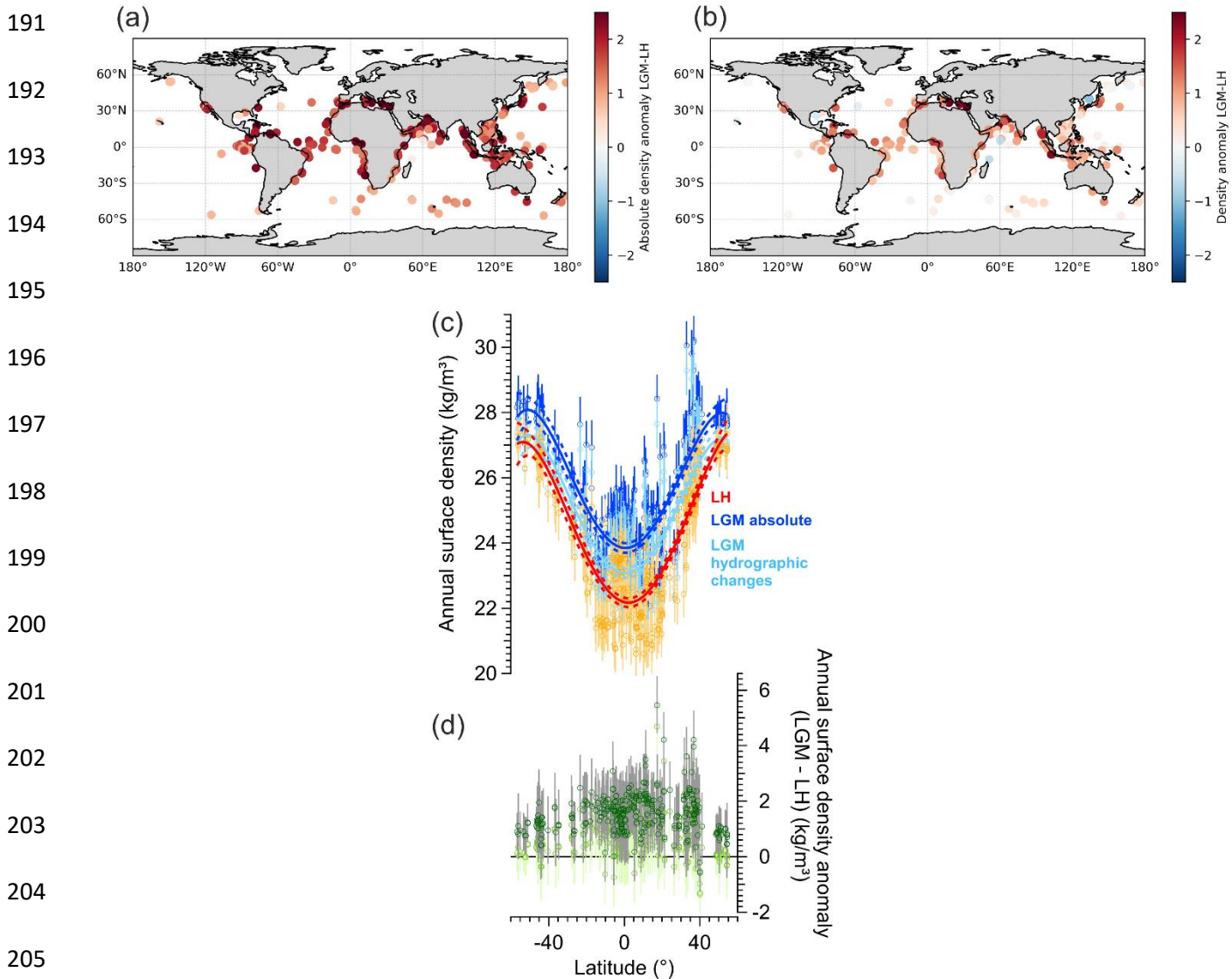
183

184 Revised Figure 6: probability distributions of surface density residuals anomaly (LGM - PI) for
 185 ECHAM5/MPI-OM and iLOVECLIM, for global data (a and c), and without the Nordic Seas and
 186 northern North Atlantic (north of 40°N) (b and d). North Indian Ocean data for iLOVECLIM
 187 have been removed in both cases.

188

189

190



207 Figure 7 revised: reconstructions of LGM and LH annual surface ocean density from
 208 foraminifera $\delta^{18}\text{O}$. (a) Spatial distribution of the LGM - LH absolute density anomaly. (b)
 209 Spatial distribution of the LGM - LH density changes due to hydrographic changes in SST and
 210 SSS. (c) Meridional gradient of reconstructed surface annual LGM density (absolute density
 211 in dark blue, density due to hydrographic changes in light blue) and comparison with LH
 212 reconstructions (red and orange colors). Error bars for each data point represent the 68 %
 213 C.I. A polynomial fit (5th degree) and associated 95% confidence bands are shown as solid
 214 resp. dashed lines. (d) Meridional gradient of reconstructed density anomaly (LGM - LH) for
 215 absolute density in dark green and density due to hydrographic changes in light green and
 216 associated 68 % C.I (grey lines).

217

218

219 **2. Uncertainty of density reconstruction.** With respect to the previous point, the uncertainty
220 in the density reconstruction due to ocean volume changes should be implemented into the
221 error analysis.

222 Based on our new analyses this uncertainty is very small (**less than 0.1 in observations and**
223 **model simulations**, see discussion before and Figure b) in comparison to uncertainties in the
224 Bayesian calibration (see Figure 2 of our paper). We performed a sensitivity test based on
225 our LGM database for three different foraminifera species. We used a method for
226 propagating uncertainty in density estimates through bootstrapping. It allows for the
227 calculation of confidence intervals (CIs) that account for this additional uncertainty
228 (estimated here to be 0.1), resulting in updated confidence intervals for the uncertainties of
229 absolute densities (Tables 1 and 2).

Species	Mean density (ρ)	CI Low 80%	CI High 80%	CI Low 95%	CI High 95%
<i>N. pachyderma</i>	25.72	25.11	26.35	24.78	26.68
<i>G. ruber</i>	24.19	23.25	25.13	22.74	25.67
<i>G. bulloides</i>	26.18	25.08	27.31	24.47	27.90

230 Table 1: initial density prediction and uncertainties for an example of three different
231 foraminifera species.

Species	Mean density (ρ)	CI Low 80%	CI High 80%	CI Low 95%	CI High 95%
<i>N. pachyderma</i>	25.72	25.09	26.36	24.75	26.72
<i>G. ruber</i>	24.19	23.21	25.16	22.71	25.69
<i>G. bulloides</i>	26.18	25.04	27.30	24.45	27.88

232
233 Table 2: density prediction and uncertainties for the same example of three different
234 foraminifera species but adding the uncertainty in the density reconstruction due to ocean
235 volume changes.

240 **Our sensitivity test of uncertainties propagation through bootstrapping indicates that the**
241 **uncertainties in the density reconstruction due to ocean volume changes can be neglected.**

242

243 With respect to the uncertainty of $\delta^{18}\text{O}$ seawater reconstructions (line 72-75), I recommend
244 citing the work of Schmidt (1999), because this author provides a reliable error estimate for
245 $\delta^{18}\text{O}$ sea water reconstructions.

246 Ok, done

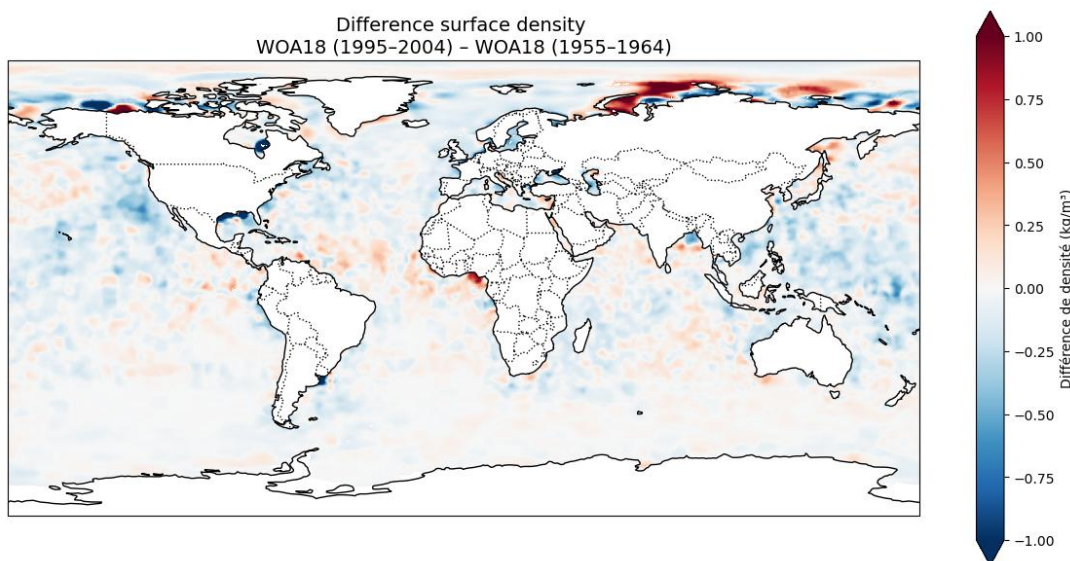
247 Also, I miss an assessment if the total error of the method is small enough to distinguish
248 glacial densities from the modern ones, particularly if the global warming bias in the modern
249 reference data is considered.

250 Uncertainties given in Figure 2 of our paper (uncertainties at 1 sigma) can be compared to
251 changes in density in our submitted or revised Figure 7. It is dependent on the species

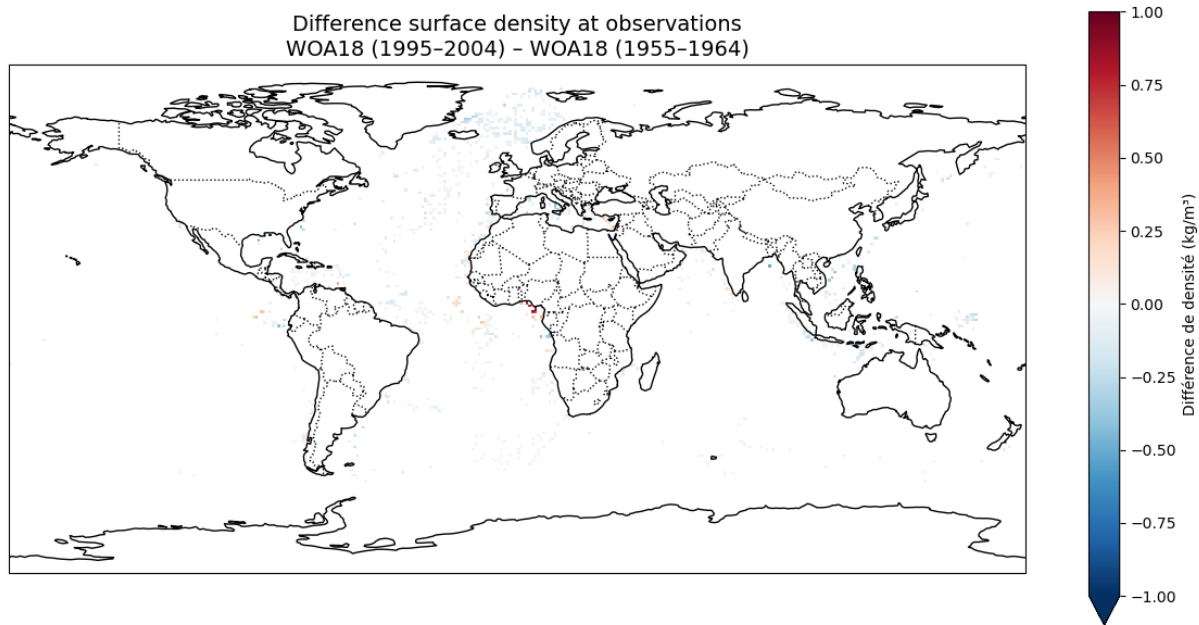
252 considered but is comprised between around 0.48 and 0.86 (at 1 sigma), for reconstructed
253 density changes due to hydrographic changes in SST and SSS (the local/regional SST and SSS
254 changes mentioned by the reviewer) that vary between around 0 and 3 and absolute density
255 changes between around 0.8 and 3.8 (see revised Figure 7). Note that when absolute density
256 is considered, the signal/noise ratio increases because density increases at the LGM (by
257 around 0.77) but the uncertainties is similar (see our estimation discussed before). **So yes,**
258 **the total error of the method is small enough to distinguish absolute glacial densities from**
259 **the modern ones.**

260 Regarding a potential global warming bias in the modern reference data.

261 For the Multi Observation Global Ocean Sea Surface density product (Droghei et al., 2016;
262 2018, cmems), we used the period 1993-2003 for our calibration but the temporal extent is
263 only from 1993 to 2025 so we cannot investigate if older historical period can lead to
264 different densities compare to a period more affected by the global warming. As suggested
265 by the reviewer in point “**8. Global warming in modern hydrography**”, **There might be**
266 **products like the World Ocean Atlas that integrate over longer time periods and therefore**
267 **contain less global warming signals.** We therefore investigate WOA18 observations and
268 compare the available periods 1995-2004 (closest period to the one we use for the
269 calibration) and the period 1955-1964, the oldest one proposed for WOA18 and susceptible
270 to be less affected by global warming effect (Figure c).

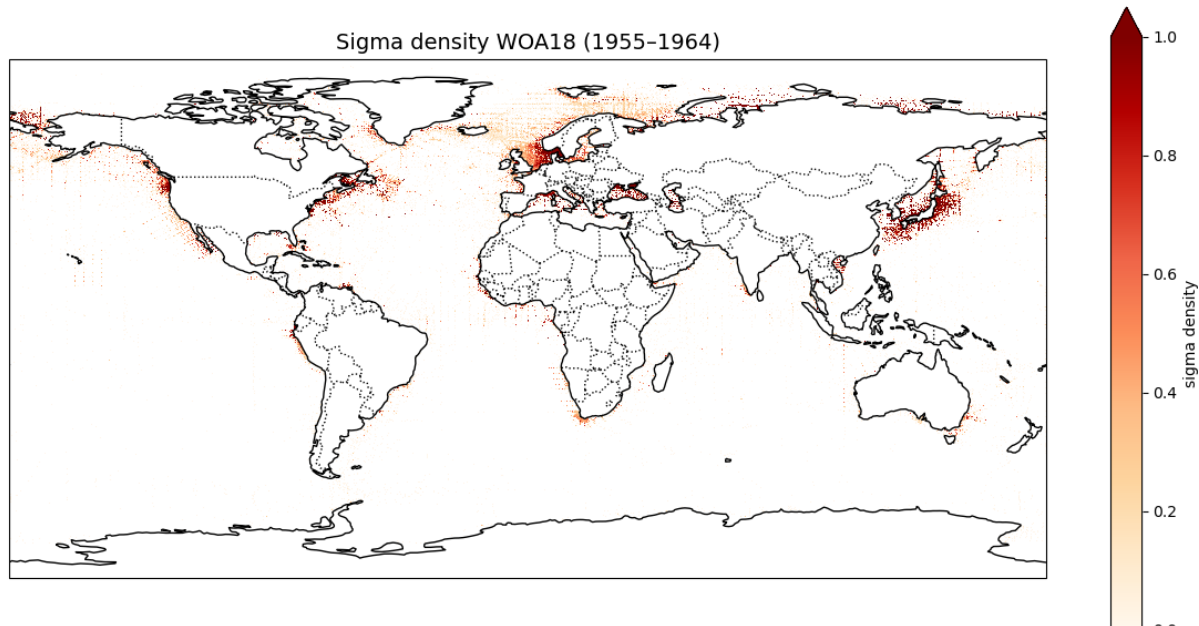


286 density product rather than a global warming effect, as highlighted in Figure e for this
287 region.



288

289 Figure d: difference in surface density (WOA18 1995-2004 – WOA18 1955-1964) at
290 observation sites.



299

301

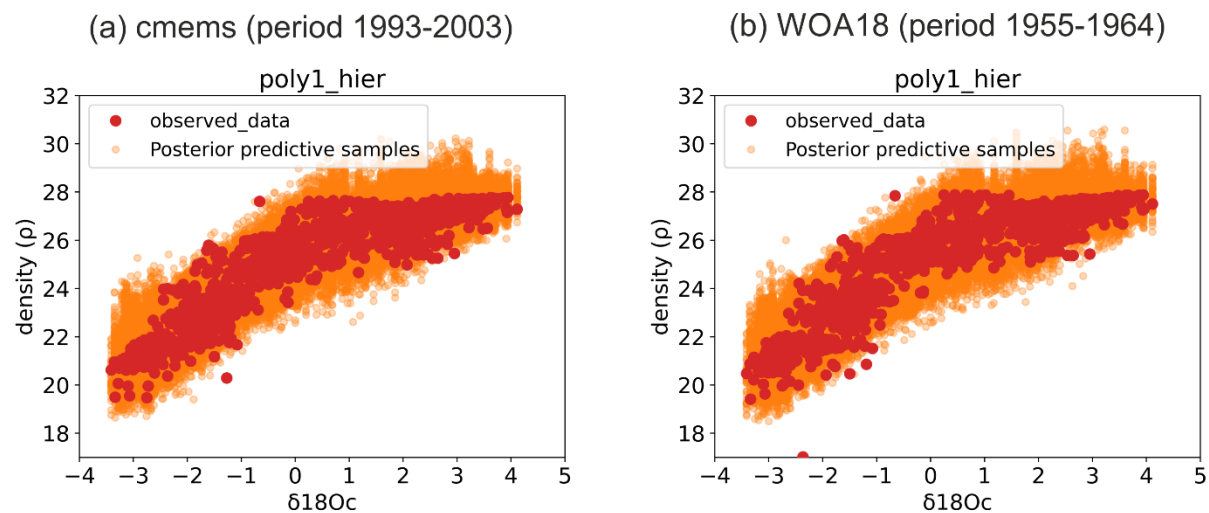
302 Figure e: The standard deviation about the statistical mean of surface density in each grid-
303 square (WOA18 1955-1964).

304

305

306 To clearly demonstrate that a potential global warming bias in the modern reference data
307 has no significant influence on our final density prediction, we realized a new Bayesian
308 calibration with WOA18 (period 1955-1964) as the modern reference data and compared it
309 with our previous calibration (cmems, period 1993-2003) (Figures f and g).

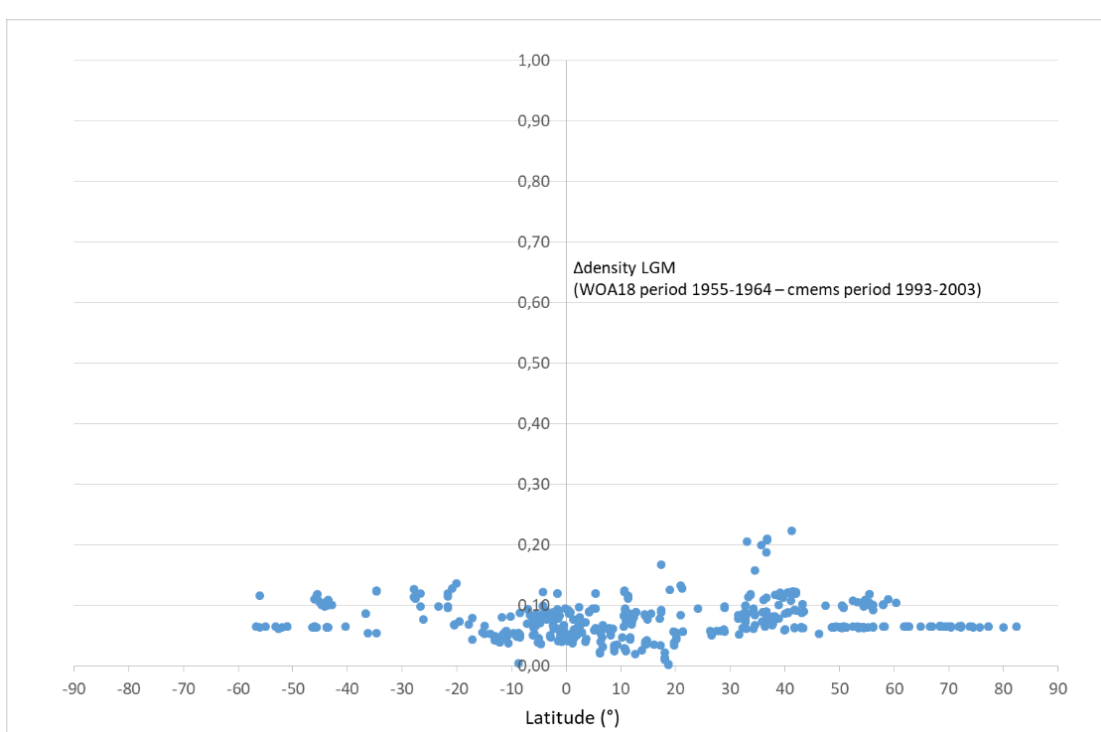
310



312

313 Figure f: Bayesian calibrations with (a) cmems density observations (period 1993-2003) and
314 (b) with WOA18 density observations (period 1955-1964).

315



317 Figure g: Difference in density at LGM predicted using WOA18 (period 1955-1964)
318 observations for the calibration – predictions using cmems observations for the calibration
319 (period 1993-2003).

320 We observe (Figures f and g) differences that are generally lower than 0.1 and of maximum
321 0.2 kg/m³. Similar results are obtained for the confidence interval calculated. As already
322 demonstrated in response to point 2 of the reviewer, these differences can be considered as
323 uncertainties that can be neglected.

324 **Therefore, the type of density product (WOA18 versus cmems observations) and the time**
325 **period considered (period 1955-1964 versus 1993-2003) have no significant impact on our**
326 **Bayesian calibration models and associated LGM density predictions within the estimated**
327 **uncertainty.**

328

329

330 **3. Ice effect correction.** The authors cite an ice effect correction of either 1.0 (line 365) or
331 1.05 (line 421). Please clarify why different numbers have been used or correct. I also find it
332 appropriate to cite Labeyrie et al. (1987) (see their Fig. 5) in this context, as they for the first
333 time provided robust evidence for an ice effect on the order of 1 o/oo.

334 Yes, we keep 1.0 %o and we added references of Schrag et al., 2002 and Labeyrie et al.
335 (1987).

336 **4. Transparency.** The documentation of the data sources is not sufficient. For the LGM
337 compilation the authors mention „additional data“ which are not specified anywhere in the
338 paper. In the „Code and data availability“ section, it is stated that „The additional LGM and
339 δ18Oc dataset will be available as a supplement“. Unfortunately, the supplement is not
340 available to me. The „Obligations to authors“ states that „A paper should contain sufficient
341 detail and references to public sources of information to permit the author's peers to
342 replicate the work.“ As a reviewer, I am unable to replicate the work because neither the
343 data/supplement nor all the sources are available to me. Also, „Copernicus Publications
344 requests depositing data that correspond to journal articles in reliable (public) data
345 repositories, assigning digital object identifiers, and properly citing data sets as individual
346 contributions“ (from https://www.climate-of-the-past.net/policies/data_policy.html). I
347 strongly suggest that the authors adhere to this policy.

348 All the data and the code for the Bayesian calibrations are freely available at the following
349 repository: https://github.com/nicrie/density_uncertainty. We refrained to share these data
350 at the stage of the preprint because the data will be publicly available but still not validated
351 and accepted for publication. We understand and agree that the reviewers should have
352 access to these data before publication. We also shared the link with the editor.

353 We revised the Code and data availability section as follows: “The Python code for Bayesian
354 calibration models is freely available at the following repository:
355 https://github.com/nicrie/density_uncertainty. Core top data used for this analysis are from

356 Malevich et al. 2019 and are available at
357 <https://agupubs.onlinelibrary.wiley.com/doi/10.1029/2019PA003576>. LGM and LH $\delta^{18}\text{O}_{\text{C}}$
358 dataset are available at doi:10.5194/cp-10-1939-2014-supplement for Caley et al., 2014, at
359 <https://doi.org/10.1594/PANGAEA.894229> for Waelbroeck et al., 2014 and at
360 <https://doi.org/10.1594/PANGAEA.920596> for Tierney et al., 2020b. The additional LGM and
361 LH $\delta^{18}\text{O}_{\text{C}}$ dataset is available at the following repository:
362 https://github.com/nicrie/density_uncertainty.”

363 **5. Transport of foraminiferal shells with currents.** Currents can transport foraminiferal
364 shells and the isotope signals they carry over relatively large distances. Based on typical
365 current speeds, it can be estimated that planktic foraminifera may be transported several
366 degrees latitude within their lifetime. While one can argue that the effects will be minimal
367 because the ambient water mass is transported with the shells, discrepancies between
368 recorded $\delta^{18}\text{O}$ and calculated $\delta^{18}\text{O}$ may occur if foraminifera/water masses are subducted, if
369 water masses are mixed or in the vicinity of fronts, with the filaments from upwelling regions
370 or close to freshwater plumes. I suggest that the authors consider and discuss shell
371 transport/expatriation in addition to seasonality and vertical migration.

372 We agree that transport of foraminifera shells by currents is one additional process that can
373 potentially lead to discrepancies between recorded $\delta^{18}\text{O}$ and calculated $\delta^{18}\text{O}$ or
374 hydrographic data. However, as mentioned by the reviewer, one can argue that the effects
375 will be minimal because the ambient water mass is transported with the shells. Indeed, our
376 comparison between simulated $\delta^{18}\text{O}_{\text{C}}$ and core tops observations (Figure 4) indicates that
377 this effect would be weak.

378 In addition, this effect is implicitly included in the uncertainty. We assume here that this is a
379 stochastic process that will lead sometimes to a positive and sometimes to a negative error,
380 which accordingly inflates the credible intervals of our predictions.

381 We propose to add a few sentences to explain this potential additional effect in the
382 paragraph dealing with all potential influences on the $\delta^{18}\text{O}_{\text{C}}$ signal in addition to
383 temperature and $\delta^{18}\text{O}_{\text{sw}}$ (lines 100-103): “Transport of foraminifera shells by currents is
384 another process that could lead to discrepancies between recorded $\delta^{18}\text{O}_{\text{C}}$ and calculated
385 $\delta^{18}\text{O}_{\text{C}}$ or hydrographic data. However, this effect is likely minimal because the ambient water
386 mass is transported together with the shells.”

387

388 **6. Abstract.** „We developed the use of the $\delta^{18}\text{O}_{\text{C}}$ of planktonic foraminifera as a surface
389 paleodensity proxy for the whole ocean...“. As the authors show obviously not for the Nordic
390 Seas and hence not for the global ocean surface.

391 Ok, we changed this for “We developed the use of the $\delta^{18}\text{O}_{\text{C}}$ of planktonic foraminifera as a
392 surface paleodensity proxy using Bayesian regression models calibrated to annual surface
393 density”.

394 **7. Effect of mixing/bioturbation (line 91-95).** The paper by Köhler and Mulitza (2024) mainly
395 deals with the detection of the carbon ion effect, not with bioturbation. Bioturbation will
396 have a significant effect on most core tops used in this study. At typical mixed layer depths
397 of 5-10 cm, deglacial/glacial material will be mixed with the Holocene layer below a
398 sedimentation rate threshold of about 2 cm/kyr (see for example Broecker, 1986), mid-
399 Holocene material (including monsoonal related salinity/density changes) at even higher
400 sedimentation rates. For most of the MARGO core tops, there seems to be a weak
401 stratigraphic control.

402 This is an issue that affects all core-top calibrations (see for example Malevich et al., 2019).
403 However, our comparison between simulated $\delta^{18}\text{O}_{\text{C}}$ and core tops observations (Figure 4)
404 indicates that this effect should be weak. If mixing/bioturbation effect was dominant, since
405 there is no bioturbation in model simulations, we would expect no agreement on Figure 4
406 ($R^2 = 0.9$).

407 In addition, this effect is implicitly included in the uncertainty. We assume here that this is a
408 stochastic process that will lead sometimes to a positive and sometimes to a negative error,
409 which accordingly inflates the confidence intervals of our predictions.

410 Moreover, the MARGO core top data set only contains cores for which bioturbation is not
411 severe. In low sedimentation cores, bioturbation would lead to the mixing of glacial and
412 interglacial shells which would in turn lead to abnormally heavy Holocene $\delta^{18}\text{O}_{\text{C}}$. In the
413 MARGO data set, sediment cores with sedimentation rates lower than 5 cm/ky were
414 discarded when planktonic $\delta^{18}\text{O}_{\text{C}}$ values were heavier than the SST vs ($\delta^{18}\text{O}_{\text{C}} - \delta^{18}\text{O}_{\text{W}}$)
415 regression value + 1 root mean square error (Waelbroeck et al., 2005).

416 We changed the text in lines 96-99 as follows: “The four processes mentioned above have
417 not been clearly demonstrated. In addition, the carbonate ion effect has been shown to have
418 no detectable influence (Köhler and Mulitza, 2024) and core top data have been selected to
419 limit the bioturbation effect (Waelbroeck et al., 2005).”

420 **8. Global warming in modern hydrography.** The fact that all core top calibrations are
421 affected by global warming (line 140) is not a good justification for its use. There might be
422 products like the World Ocean Atlas that integrate over longer time periods and therefore
423 contain less global warming signals. This issue should at least be discussed, since global
424 ocean warming approaches the magnitude of the deglacial warming and the bias can be
425 considerable.

426 This is a potential issue that affects all core-top calibrations (see for example Malevich et al.,
427 2019, Tierney et al., 2019). But see our response to point 2. To clearly demonstrate that a
428 potential global warming bias in the modern reference data has no influence on our final
429 density prediction, we realized a new Bayesian calibration with WOA18 (period 1955-1964)
430 as the modern reference data and compare with our previous calibration (cmems, period
431 1993-2003) (Figures f and g).

432 **Therefore, the type of density product (WOA18 versus cmems observations) and the time**
433 **period considered (period 1955-1964 versus 1993-2003) have no significant impact on our**

434 **Bayesian calibration models and associated LGM density predictions within the estimated**
435 **uncertainty.**

436

437 **9. Stability of the $\delta^{18}\text{O}_{\text{w}}$ salinity relationship.** The authors have tested the stability of the
438 $\delta^{18}\text{O}$ /salinity relationships with the results of model simulations for the LGM. I find the
439 choice of the time slice not ideal. In the tropics and subtropics (the majority of the ocean
440 area), the strongest precipitation changes (and hence changes in surface $\delta^{18}\text{O}$ and salinity)
441 occur in the early to mid-Holocene with the strengthening of the Monsoon (see for example
442 Weldeab et al. 2007). This is the time when I would expect changes in $\delta^{18}\text{O}$ of the freshwater
443 endmember for example due to the amount effect and hence a potential instability of the
444 $\delta^{18}\text{O}$ /Salinity relation. The authors should have access to isotope-enabled model runs
445 representing the mid-Holocene (e.g., Shi et al. 2023, co-authored by M. Werner).

446 Our work is really focus on the LGM and so testing the stability of the $\delta^{18}\text{O}$ /salinity
447 relationships for the MH and its potential effect on density predictions is rather out of the
448 scope of this paper. Nonetheless, we agree that it is interesting to put into context our
449 results regarding other climate periods. We conducted some preliminary tests using isotope-
450 enabled model runs representing the mid-Holocene (e.g., Shi et al. 2023) in order to
451 demonstrate that additional uncertainties due to the evolution of the $\delta^{18}\text{O}_{\text{c}}$ -density
452 relationship with time are globally weak and that the new calibration has great potential to
453 be applied to other past periods and to reconstruct the past temporal evolution of ocean
454 surface density over the quaternary.

455

456

457

458

459

460

461

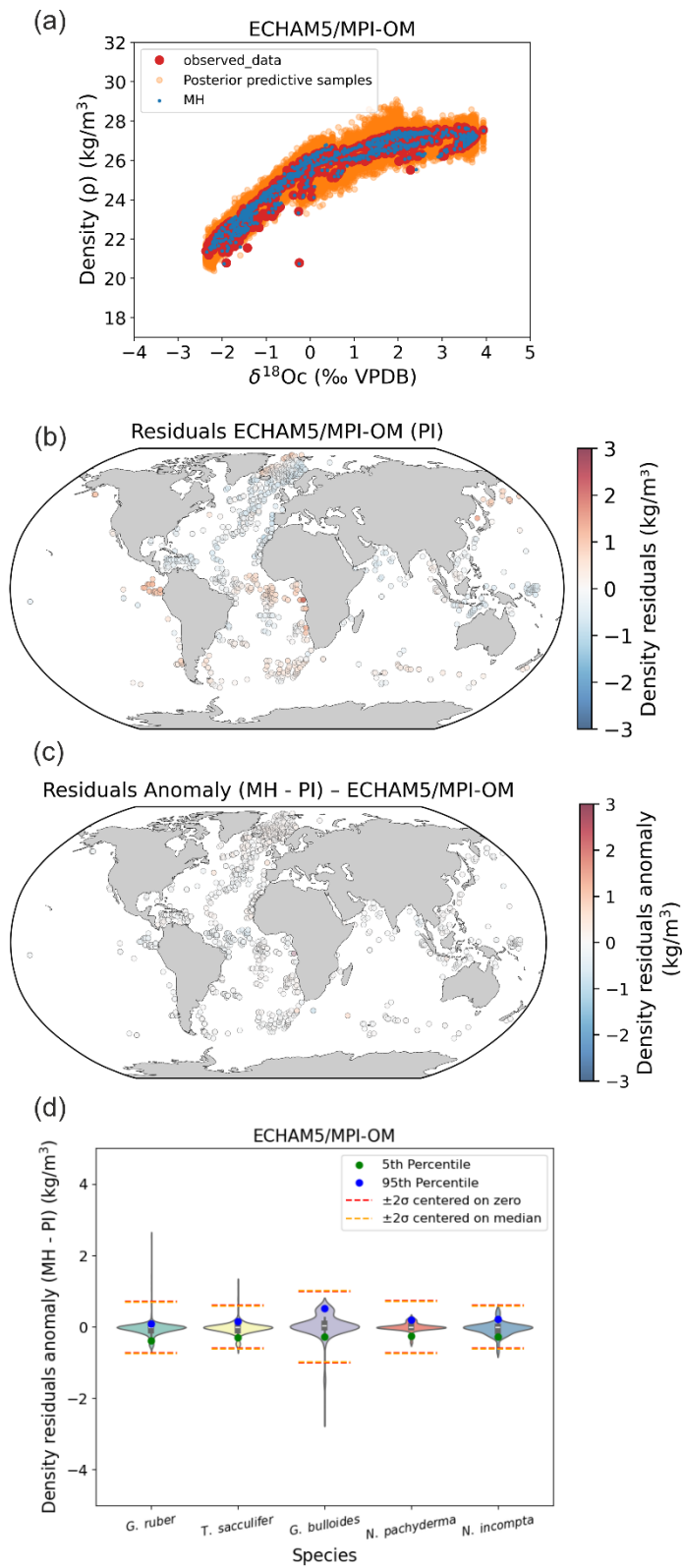
462

463

464

465

466



492 Figure h: Stability of foraminifera $\delta^{18}\text{Oc}$ -density relations between PI and the MH calculated
 493 with FAME and forced by global AWI-ESM-2.1-wiso (Shi et al., 2023) hydrographic data. (a) PI
 494 Bayesian regression models between foraminifera $\delta^{18}\text{Oc}$ and annual surface density.
 495 Posterior predictive samples and the MH $\delta^{18}\text{Oc}$ -density relation (MH) are visible. (b) Density
 496 residuals (predicted - observed) for the PI experiments. (c) Density residuals anomaly

497 between MH and PI. (d) Probability distributions of surface density residuals anomaly (MH -
498 PI) without Nordic Seas (north of 40°N).

499 Results of the Figure h clearly indicates a strong stability of foraminifera $\delta^{18}\text{O}$ -density
500 relations between MH and the PI and so very weak influence of $\delta^{18}\text{O}$ /Salinity relation
501 instability on final density predictions.

502 These results are now part of the new “Appendix B. Application of our calibration to other
503 past periods”.

504 **10. Direct comparison to modelled LGM density.** Why has the LGM foraminiferal-based
505 density reconstruction not directly been compared to modelled LGM density? The models
506 are considered good enough to test the stability of the $\delta^{18}\text{O}$ salinity relation, why are they
507 not good enough to compare with the density reconstruction directly?

508 This will be the focus of a detailed paper submitted very soon Barathieu et al.,. As mentioned
509 in our paper in line 439-440: “Further regional analyses of ocean surface density and
510 comparison with numerical climate models are presented in Barathieu et al. in prep.”

511 We think that it would be interesting to have this detailed data-model comparison paper as
512 a companion paper of our paper in CP if the editor agrees.

513 We present some results of data-model comparison from the paper of Barathieu et al., that
514 will be submitted soon to show that the models used in our study (MPI and iLOVECLIM)
515 exhibit significant (p-value <0.05) and strong correlation ($R^2>0.5$) with our reconstructed
516 density for the PI and LGM (see response to reviewer 2 for details).

517

518

519

520 Broecker, W. S.: Oxygen Isotope Constraints on Surface Ocean Temperatures, *Quat. res.*, 26,
521 121–134, [https://doi.org/10.1016/0033-5894\(86\)90087-6](https://doi.org/10.1016/0033-5894(86)90087-6), 1986.

522 Duplessy, J.-C., Labeyrie, L., Anne, Maitre, F., Duprat, J., and Sarnthein, M.: Surface salinity
523 reconstruction of the North Atlantic Ocean during the LGM, *Oceanologica Acta*, 14, 311–324,
524 1991.

525 Labeyrie, L. D., Duplessy, J. C., and Blanc, P. L.: Variations in mode of formation and
526 temperature of oceanic deep waters over the past 125,000 years, *Nature*, 327, 477–482,
527 <https://doi.org/10.1038/327477a0>, 1987.

528 Köhler, P. and Mulitza, S.: No detectable influence of the carbonate ion effect on changes in
529 stable carbon isotope ratios ($\delta^{13}\text{C}$) of shallow dwelling planktic foraminifera over the past
530 160 kyr, *Clim. Past*, 20, 991–1015, <https://doi.org/10.5194/cp-20-991-2024>, 2024.

531 Schmidt, G. A.: Error analysis of paleosalinity calculations, *Paleoceanography*, 14, 422–429,
532 <https://doi.org/10.1029/1999PA900008>, 1999.

533 Shi, X., Cauquoin, A., Lohmann, G., Jonkers, L., Wang, Q., Yang, H., Sun, Y., and Werner, M.:
534 Simulated stable water isotopes during the mid-Holocene and pre-industrial periods using
535 AWI-ESM-2.1-wiso, *Geosci. Model Dev.*, 16, 5153–5178, <https://doi.org/10.5194/gmd-16-5153-2023>, 2023.

537 Weldeab, S., Lea, D. W., Schneider, R. R., and Andersen, N.: 155,000 years of West African
538 monsoon and ocean thermal evolution, *Science (New York, N.Y.)*, 316, 1303–1307,
539 <https://doi.org/10.1126/science.1140461>, 2007.

540 References:

541 Droghei, R., Nardelli, B. B., and Santoleri, R.: Combining In Situ and Satellite Observations to
542 Retrieve Salinity and Density at the Ocean Surface, *J. Atmos. Ocean. Tech.*, 33, 1211–1223,
543 <https://doi.org/10.1175/JTECH-D-15-0194.1>, 2016.

544 Droghei, R., Buongiorno Nardelli, B., and Santoleri, R.: A new global sea surface salinity and
545 density dataset from multivariate observations (1993–2016), *Frontiers in Marine Science*, 5,
546 <https://doi.org/10.3389/fmars.2018.00084>, 2018.

547 Malevich, S. B., Vetter, L., and Tierney, J. E.: Global core top calibration of $\delta^{18}\text{O}$ in planktic
548 foraminifera to sea surface temperature, *Paleoceanogr. Paleoclimatol.*, 34, 1292–1315,
549 2019.

550 Schrag, D. P., Adkins, J. F., McIntyre, K., Alexander, J. L., Hodell, D. A., Charles, C. D., &
551 McManus, J. F. (2002). The oxygen isotopic composition of seawater during the Last Glacial
552 Maximum. *Quaternary Science Reviews*, 21(1-3), 331-342.

553

554 Tierney, J. E., Malevich, S. B., Gray, W., Vetter, L., & Thirumalai, K. (2019). Bayesian
555 calibration of the Mg/Ca paleothermometer in planktic foraminifera. *Paleoceanography and*
556 *Paleoclimatology*, 34(12), 2005-2030.

557

558 Tierney, J. E., Zhu, J., King, J., Malevich, S. B., Hakim, G. J., & Poulsen, C. J. (2020). Glacial
559 cooling and climate sensitivity revisited. *Nature*, 584(7822), 569-573.

560

561 Waelbroeck, C., Mulitza, S., Spero, H., Dokken, T., Kiefer, T., and Cortijo, E.: A global
562 compilation of Late Holocene planktic foraminiferal $\delta^{18}\text{O}$: Relationship between surface
563 water temperature and $\delta^{18}\text{O}$, *Quaternary Sci. Rev.* 24, 853–878, 2005.

564

565

566

567

568 **Response to Reviewer 2**

569 **General comment**

570 Caley et al. investigate the use of planktonic foraminifera $\delta^{18}\text{O}_c$ as a surface paleodensity proxy
571 for the whole ocean. For that, the authors applied three Bayesian regression models on
572 $\delta^{18}\text{O}_c$ datasets to reconstruct surface paleodensity for the late Holocene (LH) and the Last
573 Glacial Maximum (LGM). Using isotope-enabled models of different complexities, Caley et al.
574 investigated the additional uncertainties that are introduced by the potential evolution of
575 the $\delta^{18}\text{O}_c$ -density relationship with time (i.e., from LGM to LH). Except for the Nordic Seas,
576 the authors demonstrated that additional uncertainties are weak globally (for a LGM to LH
577 climate change).

578 The objectives and the method of this study correspond to the scope of CP. The study is easy
579 to follow, and I took pleasure to read it. I have some minor comments related to the
580 datasets, the evaluation, and the comparison with LGM results.

581

582 **Major comments**

583 • The description of the LGM $\delta^{18}\text{O}$ dataset lacks details, especially, on the additional
584 data from more recent studies (lines 130-131), which are not available with the paper
585 (or I missed them). For the revised paper, I suggest the reviewer to provide the
586 compilation of all the data ($\delta^{18}\text{O}$ for LH and LGM + ocean datasets) they used for this
587 study, with the appropriate references inside.

588 All the data and the code for the Bayesian calibrations are freely available at the following
589 repository: https://github.com/nicrie/density_uncertainty. We refrained to share these data
590 at the stage of the preprint because the data will be publicly available but still not validated
591 and accepted for publication. We understand and agree that the reviewers should have
592 access to these data before publication. We also shared the link with the editor.

593 The additional dataset from more recent studies is freely available at
594 https://github.com/nicrie/density_uncertainty but the previously published $\delta^{18}\text{O}$ data for LH
595 and LGM are already available to download on the original repository in the “code and data
596 availability” part: “LGM and LH $\delta^{18}\text{O}_c$ dataset are available at doi:10.5194/cp-10-1939-2014-
597 supplement for Caley et al., 2014, at <https://doi.org/10.1594/PANGAEA.894229> for
598 Waelbroeck et al., 2014 and at <https://doi.org/10.1594/PANGAEA.920596> for Tierney et al.,
599 2020b.”

600 We consider that it is important to keep the original datasets, references and citations of
601 these previous studies as we did not change/reworked these datasets.

602 We revised the Code and data availability section as follows: “The Python code for Bayesian
603 calibration models is freely available at the following repository:
604 https://github.com/nicrie/density_uncertainty. Core top data used for this analysis are from
605 Malevich et al. 2019 and are available at

606 <https://agupubs.onlinelibrary.wiley.com/doi/10.1029/2019PA003576>. LGM and LH $\delta^{18}\text{O}$
607 dataset are available at doi:10.5194/cp-10-1939-2014-supplement for Caley et al., 2014, at
608 <https://doi.org/10.1594/PANGAEA.894229> for Waelbroeck et al., 2014 and at
609 <https://doi.org/10.1594/PANGAEA.920596> for Tierney et al., 2020b. The additional LGM and
610 LH $\delta^{18}\text{O}$ dataset is available at the following repository:
611 https://github.com/nicrie/density_uncertainty."

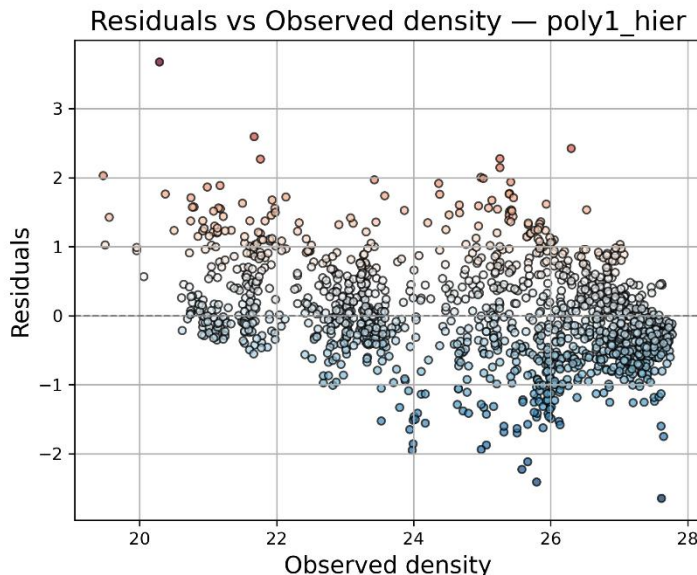
612 The full density dataset re-gridded onto a common $1^\circ \times 1^\circ$ spatial grid will be published and
613 available in the Barathieu et al. paper.

614

615 • For the evaluation of the residuals under LH climate (Figure 1), why is there a like a
616 threshold in observed data at a value of 28. Is it a problem with the data? I think it
617 should be discussed because it gives the largest density residuals. Moreover, the
618 authors do not discuss the strongest residuals in the Mediterranean Sea, which are
619 probably influenced by bias in net freshwater fluxes and thermoaline circulation. The
620 authors could use this recent study from Ayache et al. (2024,
621 <https://doi.org/10.5194/gmd-17-6627-2024>).

622 Thank you for bringing the interesting study of Ayache et al., 2024 to our attention. The
623 "threshold" in observed data at a value of 28 for density is because we are close to the
624 maximum of present day's annual ocean density. In some high latitudes regions (Nordic Seas
625 and Austral Ocean), density is already high and **temperature changes have a smaller effect**.
626 Cold water is already dense, so cooling it further doesn't increase density as much.
627 Consequently, we observe a **sensitivity decreases**. The rate of change of density with respect
628 to T flattens out, meaning the system becomes less responsive (see also our response to
629 reviewer 3). However, the density residuals are not the largest in these specific regions for
630 the poly1_hier Bayesian model as visible on (Fig. 1f) and on the Figure (a).

631 We added sentences in the text to clarify this point in lines 243-252: "We observe a
632 saturation of density values close to 28 in the calibrations that correspond to high latitudes
633 regions (Nordic Seas and Austral Ocean). When density is already high, temperature changes
634 have a smaller effect. Cold water is already dense, so cooling it further doesn't increase
635 density as much. Consequently, we observe a sensitivity decrease. The rate of change of
636 density with respect to temperature flattens out, meaning that the system becomes less
637 responsive to temperature changes. Small changes in temperature and salinity no longer
638 cause significant shifts in density. This behavior reflects to the non-linearity of the seawater
639 equation of state. Although the regression becomes less predictive in this range, the
640 estimated density values remain correct and are not expected to change strongly as ocean
641 surface density approaches its upper limits."



642

643 Figure a: Scatter plot between observed density and residuals for the poly1_hier Bayesian
 644 model. Density in kg/m³.

645 Regarding “**the strongest residuals in the Mediterranean Sea**”. According to the poly1_hier
 646 Bayesian model (Fig. 1b), there are a few points with strong residuals in its eastern part only.

647 We added a few sentences to explain that part of the Mediterranean Sea is characterized by
 648 high residuals, and propose future research improvements in lines 310-319: “Strong negative
 649 residuals are also observed in the eastern part of the Mediterranean Sea. Malevich et al.
 650 2019 reported reduced performance of their hierarchical seasonal calibration model for
 651 $\delta^{18}\text{Oc}$ and SST in this region and attributed it to the unusual behavior of *G. ruber*, potentially
 652 linked to depth-habitat migration. But estimation of seasonality for this region could also be
 653 problematic and play a role as highlighted in the study of Ayache et al. 2024. Alternatively,
 654 biases in Mediterranean net freshwater fluxes and thermohaline circulation could affect late
 655 Holocene $\delta^{18}\text{Oc}$ values (Ayache et al., 2014). Future modelling developments, such as the
 656 use of high-resolution regional model in combination with the FAME module, could help to
 657 better understand the relation between $\delta^{18}\text{Oc}$, density, temperature and $\delta^{18}\text{Osw}$ during past
 658 climate changes in the Mediterranean Sea.”

659

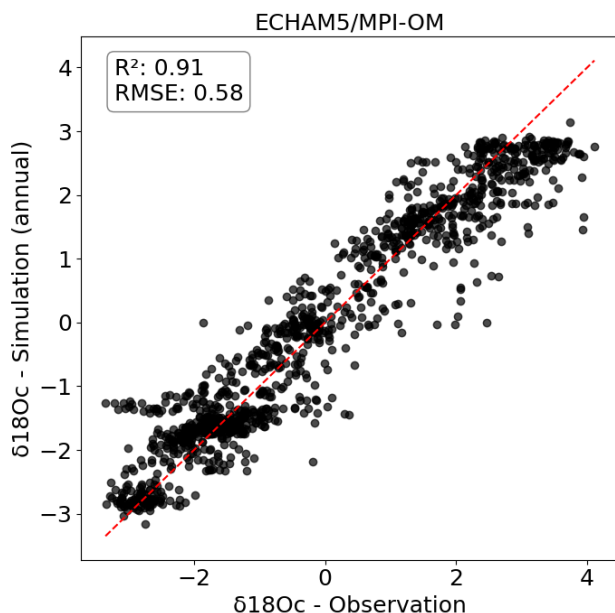
660 • Lines 328-329: I suggest to try with the yearly $\delta^{18}\text{Osw}$ values from ECHAM5/MPI-OM
 661 to really know the effect of seasonality on calculated $\delta^{18}\text{Oc}$. With the current
 662 comparison, it be cannot excluded that the differences between the results using
 663 ECHAM5/MPI-OM and iLOVECLIM is due to lower resolution of iLOVECLIM or other
 664 missing/biased processed in this lower resolution model.

665 As suggested by the reviewer, we used the ECHAM5/MPI-OM yearly values of $\delta^{18}\text{Osw}$ to
 666 compute the $\delta^{18}\text{Oc}$ (see Figure b) and compared the results with our Figure 4 (a) to better
 667 assess the effect of seasonality. Results indicate a slight decrease of the R^2 of 0.02 and a
 668 slight increase in RMSE of 0.06 when seasonality is not taken into account. To assess

669 whether the difference in predictive performance between the two models was statistically
670 significant, a paired t-test was conducted using cross-validated R^2 and RMSE scores. The test
671 yielded a t-statistic of -5.51 and a p-value of 0.0053 for R^2 (and of 5.27 with a p-value of
672 0.0062 for RMSE), indicating a significant difference between the models. Therefore,
673 seasonality partly explains the weak difference between the results using ECHAM5/MPI-OM
674 and iLOVECLIM. Lower resolution of iLOVECLIM or other missing/biased processes in this
675 model could also contribute to this weak difference.

676 We added this in the text in lines 378-385: "We tested this hypothesis by using yearly
677 ECHAM5/MPI-OM values to compute the $\delta^{18}\text{O}_{\text{C}}$ and compared the results with those
678 obtained with seasonal values (shown in Figure 4a) and better assess the effect of
679 seasonality. Results indicate a slight decrease of the R^2 of 0.02 and a slight increase in RMSE
680 of 0.06 when seasonality is not taken into account. These differences are significant
681 according to paired t-tests. Therefore, seasonality partly explains the small difference
682 between the results using ECHAM5/MPI-OM and iLOVECLIM. Lower resolution of iLOVECLIM
683 or other missing/biased processes in this model could also contribute to this small
684 difference. »

685



686

687 Figure b: comparison between PI simulated foraminifera $\delta^{18}\text{O}_{\text{C}}$ (‰) (FAME module forced
688 with yearly ECHAM5/MPI-OM climate model hydrographic data) and observed core-top
689 $\delta^{18}\text{O}_{\text{C}}$ (‰) data. The 1:1 line is indicated.

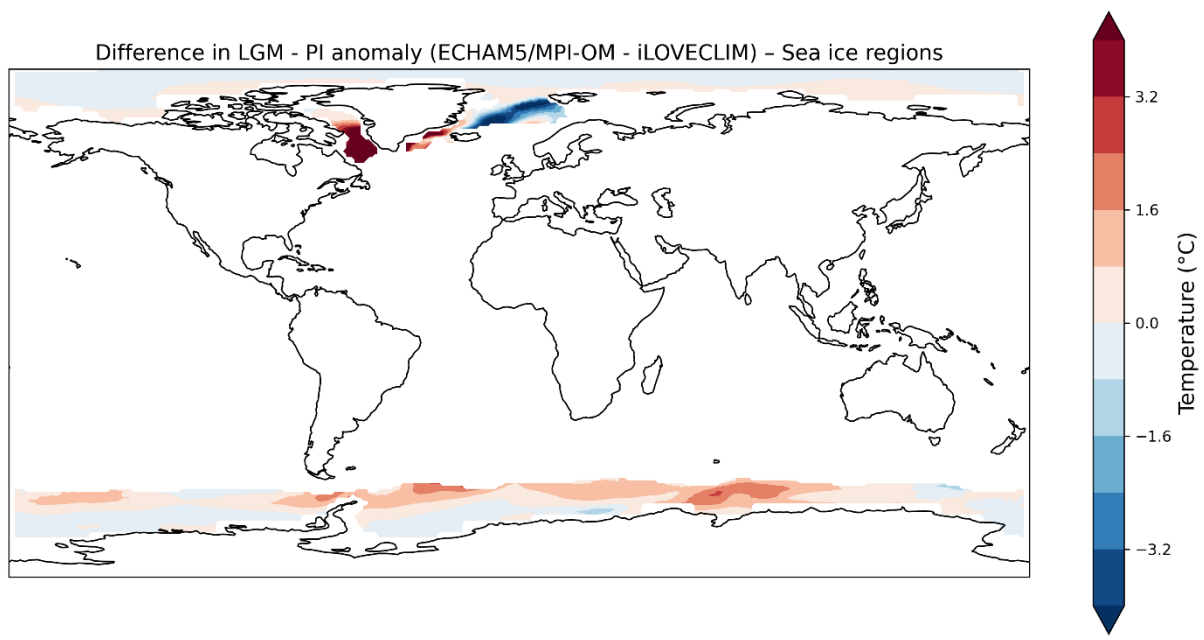
690 • For the evaluation for LGM results, the residuals in the Nordic Seas are stronger with
691 ECHAM5/MPI-OM than with iLOVECLIM (Figure 5). This point should be discussed
692 more in details by the authors.

693 The stronger difference in LGM – PI surface density anomaly residuals between
694 ECHAM5/MPI-OM and iLOVECLIM in the Nordic Seas could be explained by different

695 simulated sea ice coverage in ECHAM5/MPI-OM vs. iLOVECLIM (Figure c). Indeed, Nordic
696 seas are the region with the largest difference of modeled annual SST below 0°C.

697 Temperature is used to calculate the $\delta^{18}\text{O}$ signal, ocean density and to force the FAME
698 module. The PI $\delta^{18}\text{O}$ -density relationship is used to reconstruct LGM density based on LGM
699 $\delta^{18}\text{O}$. Then the reconstructed density is compared with modelled LGM density and so any
700 temperature differences in the Nordic seas (as visible in Figure c) will affect density
701 reconstructions and then the density residuals observed in Figure 5.

702 We added few sentences in the text to clarify this point in lines 460-468: "We also observe in
703 this region larger surface density residuals anomalies (LGM – PI) with ECHAM5/MPI-OM than
704 with iLOVECLIM (Figure 5c and f). This can be explained by different simulated sea ice
705 coverage in ECHAM5/MPI-OM compared to iLOVECLIM. Indeed, the Nordic Seas is the region
706 with the largest difference between the two model simulations of modeled annual SST
707 below 0°C (<https://doi.org/10.5194/egusphere-2025-2459-AC2>). Temperature is used to
708 calculate the $\delta^{18}\text{O}$ signal, ocean density and to force the FAME module. Any temperature
709 difference in the Nordic Seas thus affects density reconstructions and hence the density
710 residuals (Figure 5c and f). »



712 Figure c: Difference in LGM – PI anomaly between ECHAM5/MPI-OM and iLOVECLIM for SST.
713 Only region with modeled annual SST below 0°C are shown to investigate differences linked
714 to simulated sea ice coverage.

715 **Moreover, I would like to see some evaluation of the reconstructed density anomalies**
716 **between LGM and LH (Figure 7a). Are there other reconstructions? Or can the authors**
717 **compare those results with modeled LGM-LH surface densities?**

718 To our knowledge, there is no method that would provide a direct quantitative
719 reconstruction of ocean density at the global scale. Some methods exist based on dinocyst
720 assemblages, using transfer functions (see for example "Peyron, O., & Vernal, A. D. (2001).

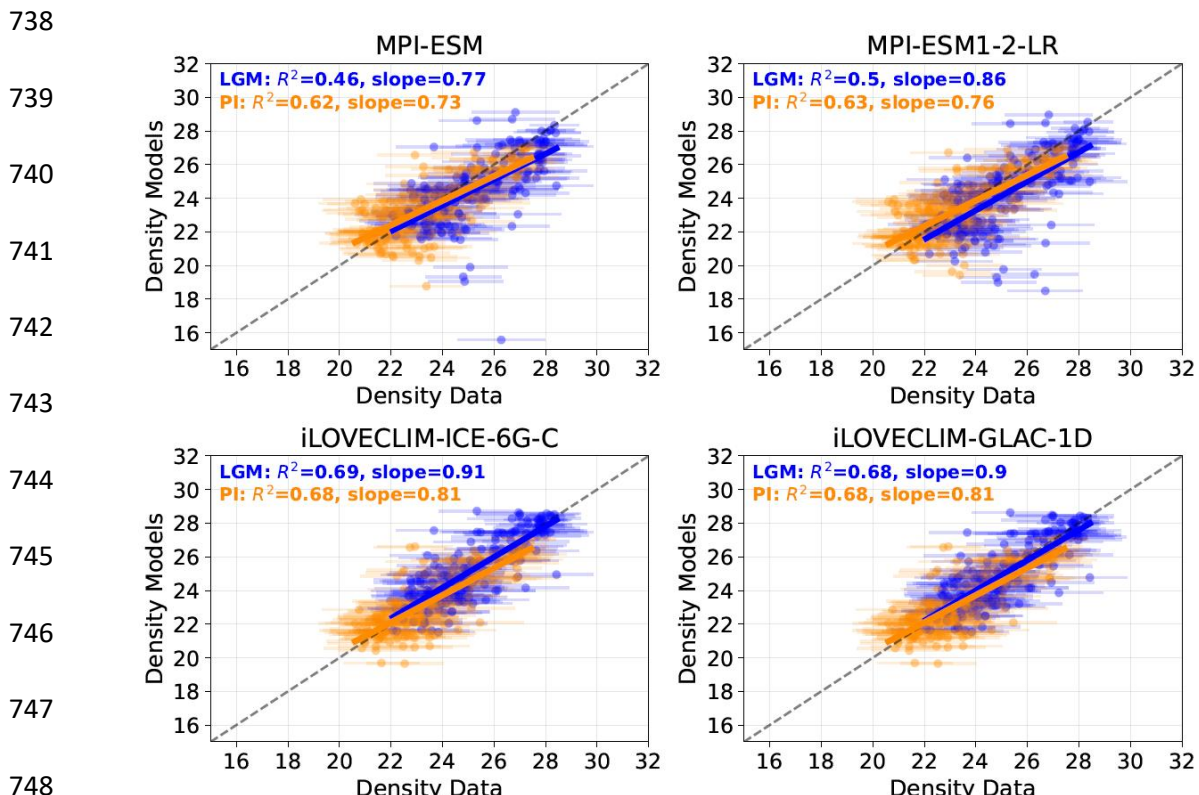
721 Application of artificial neural networks (ANN) to high-latitude dinocyst assemblages for the
722 reconstruction of past sea-surface conditions in Arctic and sub-Arctic seas. *Journal of*
723 *Quaternary Science: Published for the Quaternary Research Association*, 16(7), 699-709.”)
724 but these reconstructions are limited to the arctic regions, where we cannot evaluate our
725 reconstructed densities.

726 This lack of method at the global scale to quantitatively reconstruct densities was one of our
727 main motivations to develop our work.

728 Our results can be compared with modeled LGM-LH surface densities and this will be the
729 focus of a follow-up study by Barathieu et al. that will be submitted very soon, as mentioned
730 in our paper in line 439-440: “Further regional analyses of ocean surface density and
731 comparison with numerical climate models are presented in Barathieu et al. in prep.”

732 We think that it would be interesting to have this data-model comparison paper as a
733 companion paper of this paper in CP if the editor agrees.

734 We present some results (Figure d) of data-model comparison from the paper of Barathieu
735 et al., that will be submitted very soon to show that the models used in our study (MPI and
736 iLOVECLIM) show significant (p-value <0.05) and strong correlation ($R^2>0.5$) with our
737 reconstructed density for the PI and LGM.



749 Figure d: Linear regressions between absolute surface density from proxy-based
750 reconstructions (x-axis) and model simulations (y-axis), at the global scale. Results are shown
751 for the LGM period (blue) and the PI period (orange). Error bars on the x-axis represent the

752 95% confidence intervals of the reconstructed values. Based on Barathieu et al. in
753 preparation.

754

755 • I would like the authors to put into context their results regarding other climate
756 periods. The authors state that additional uncertainties due to the evolution of the
757 $\delta^{18}\text{O}_c$ -density relationship with time are globally weak (lines 45-46). However, this is
758 true, except for the Nordic Seas, for a LGM-to-LH change. It has not been proven for
759 another period, such as the Last Interglacial (110-130 ka). Considering mid-Holocene
760 period (6 ka) raised by the reviewer #1, the changes in $\delta^{18}\text{O}$ of seawater are rather
761 small (+0.5‰ maximum, only, in the western Pacific Ocean according to Shi et al.,
762 2023 and Cauquoin et al., 2019) compared to the LGM ones.

763 Our work is really focus on the LGM and so testing the stability of the $\delta^{18}\text{O}$ /salinity
764 relationships for the Last Interglacial (LIG) or MH (as asked by reviewer 1) and its potential
765 effect on density predictions is rather out of the scope of this paper. Nonetheless, we agree
766 that it is interesting to put into context our results regarding other climate periods. We
767 already conducted some tests using isotope-enabled model runs representing the mid-
768 Holocene (e.g., Shi et al. 2023) in order to demonstrate that additional uncertainties due to
769 the evolution of the $\delta^{18}\text{O}_c$ -density relationship with time are globally weak and that the new
770 calibration has great potential to be applied to other past periods and to reconstruct the
771 past temporal evolution of ocean surface density. **Results indicate a strong stability of**
772 **foraminifera $\delta^{18}\text{O}_c$ -density relations between MH and the PI and so very weak influence of**
773 **$\delta^{18}\text{O}$ /Salinity relation instability on final density predictions.**

774 We also test the LIG time period as asked by reviewer 2. We use isotope-enabled model runs
775 representing the LIG at 125 kyr (e.g., corresponding to the maximum changes observed
776 during the LIG period according to Figure 9 of Gierz et al., 2017) (Figure e).

777 Again results **indicate a strong stability of** foraminifera $\delta^{18}\text{O}_c$ -density relations between LIG
778 and the PI and so very weak influence of $\delta^{18}\text{O}$ /Salinity relation instability on final density
779 predictions (Figure e). **This confirms and reinforces our conclusion that the new calibration**
780 **has great potential to be applied to other past periods and to reconstruct the past**
781 **temporal evolution of ocean surface density.**

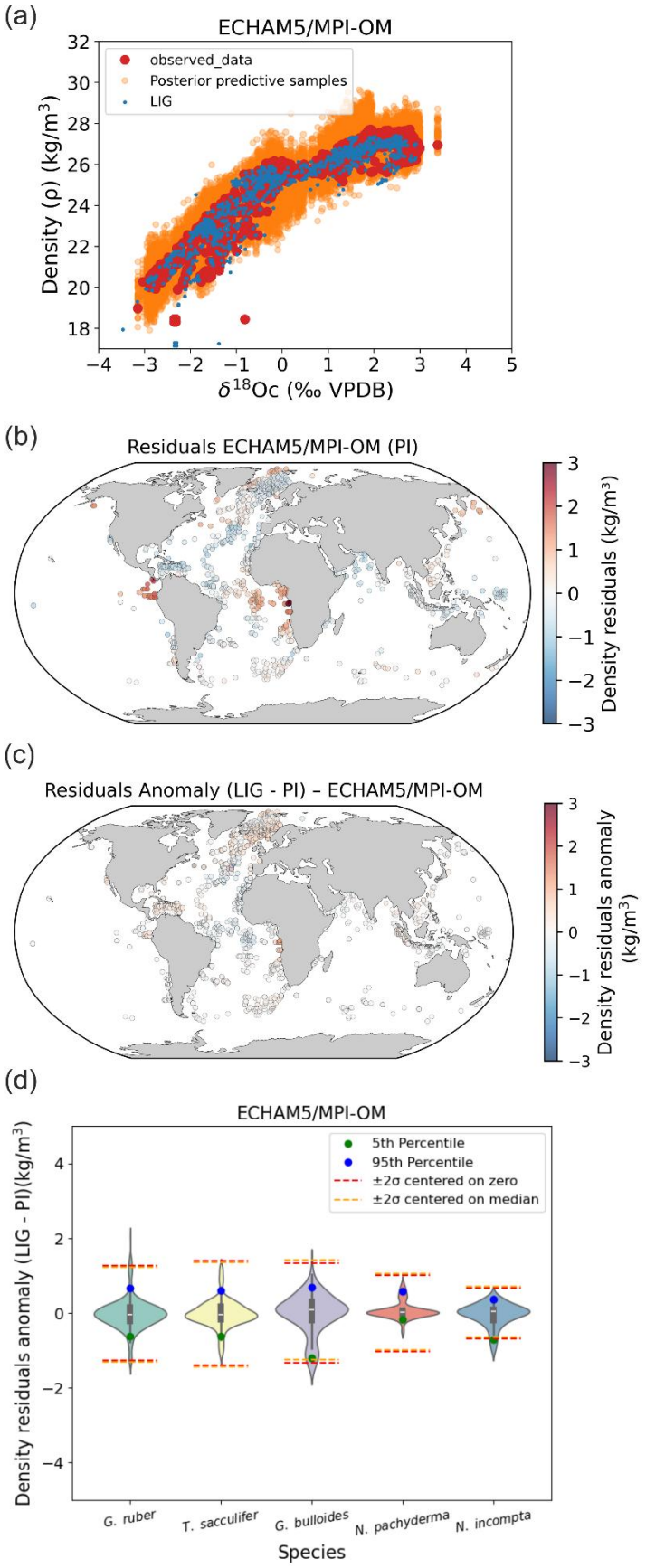
782 The additional tests we conducted during the review process for the MH and LIG time
783 periods allow us to put our results regarding other climate periods into context. We
784 therefore included these results in a new appendix (“Appendix B. Application of our
785 calibration to other past periods”) in the revised version, together with an explanatory text
786 to support and reinforce our conclusion about the new calibration and its applicability to
787 other past periods.

788

789

790

791 (a) ECHAM5/MPI-OM
792
793
794
795
796
797 (b) Residuals ECHAM5/MPI-OM (PI)
798
799
800
801
802 (c) Residuals Anomaly (LIG - PI) - ECHAM5/MPI-OM
803
804
805
806
807 (d) ECHAM5/MPI-OM
808
809
810
811
812
813
814



815

816 Figure e: Stability of foraminifera $\delta^{18}\text{O}_c$ -density relations between PI and the LIG calculated
817 with FAME and forced by global ECHAM5/MPI-OM (Gierz et al., 2017) hydrographic data. (a)
818 PI Bayesian regression models between foraminifera $\delta^{18}\text{O}_c$ and annual surface density.
819 Posterior predictive samples and LIG $\delta^{18}\text{O}_c$ -density relations (LIG) are visible. (b) Density
820 residuals (predicted - observed) for the PI experiments. (c) Density residuals anomaly
821 between LIG and PI. (d) Probability distributions of surface density residuals anomaly (LIG -
822 PI) without Nordic Seas (north of 40°N).

823

824 • Generally, the units are missing in the labels of figures' axes. Please check all the
825 figures. Also, the panel labels are used on one complete column or row in Figures 1,
826 3, 5, 6 or are absent for Figure 4. Please add a letter label for each panel in the
827 figures.

828 Ok, we corrected this in the revised version.

829 **Specific comments**

830 • Lines 74-75: to quantify past ocean density and dynamics.

831 We corrected in the revised version.

832 • Lines 148: give the units for $\delta^{18}\text{O}_c$ (and relative to which standard) and ρ (sigma-theta
833 relative to a density of 1029 kg/m³?).

834 We changed for: “ $\delta^{18}\text{O}_c$ (‰ VPDB), and annual mean surface density, ρ (kg/m³ relative to
835 water density of 1000 kg/m³)”

836 • Section 2.4.1: specify that iLOVECLIM is an intermediate-complexity model, whereas
837 ECHAM5/MPI-OM is an Earth System Model.

838 To be precise, we mention in the revised version “The iLOVECLIM (version 1.1.3) earth
839 system model of intermediate-complexity” and “use the ECHAM5/MPIOM coupled General
840 Circulation Model (GCM)”.

841 • Figure 1: This is for LH period I suppose?

842 Yes, we revised for “Bayesian calibration models for late Holocene core-top samples against
843 observed density”

844 • Lines 235: explain a bit more that is ELPD.

845 The ELPD measures the expected predictive accuracy of a Bayesian model. It is defined as
846 the sum over all data points of the expected log posterior predictive density (see Equation
847 (2) in Gelman et al. (2014)). In plain words, one could say that the ELPD is the average log

848 probability that a Bayesian model assigns to new data, summed across observations. So, in
849 our case, a higher ELPD means the model makes sharper and more accurate density
850 predictions. More details can be found in Gelman et al. (2014).

851 We added in the revised version in lines 189-193: « The ELPD measures the expected
852 predictive accuracy of a Bayesian model. It is defined as the sum over all data points of the
853 expected log posterior predictive density (Gelman et al., 2014). In our case, a higher ELPD
854 means the model makes sharper and more accurate density predictions.»

855 • **Figure 3: give the p-values.**

856 p-values have been added in the revised Figure 3 and revised text.

857 • **Figure 4: Only for LH period?**

858 We specified this in the revised version: “comparison between simulated PI foraminifera
859 $\delta^{18}\text{O}_{\text{C}}$ (FAME module forced with ECHAM5/MPI-OM and iLOVECLIM climate model
860 hydrographic data) and observed LH core-top $\delta^{18}\text{O}_{\text{C}}$ data. The 1:1 line is indicated.”

861 • **Row (a) of Figure 5: the legend for the LGM values is not clear.**

862 We specified in the revised legend of the Figure 5: “the LGM $\delta^{18}\text{O}_{\text{C}}$ -density relations (LGM)
863 are visible”

864 • **Line 421: 1 or 1.05‰?**

865 Yes, we keep 1.0 ‰ and we added references of Schrag et al., 2002 and Labeyrie et al.
866 (1987) in agreement with reviewer 1’s comment.

867 • **Lines 455-456: By applying a Bayesian regression hierarchical model to LGM and LH
868 $\delta^{18}\text{O}_{\text{C}}$ foraminifera databases, we reconstructed LGM and LH annual surface density
869 and found stronger LGM density...**

870 We corrected in the revised version

871 **References**

872 Ayache, M., Dutay, J.-C., Mouchet, A., Tachikawa, K., Risi, C., and Ramstein, G.: Modelling the
873 water isotope distribution in the Mediterranean Sea using a high-resolution oceanic model
874 (NEMO-MED12-watiso v1.0): evaluation of model results against in situ observations, *Geosci.
875 Model Dev.*, **17**, 6627–6655, <https://doi.org/10.5194/gmd-17-6627-2024>, 2024.

876 Cauquoin, A., Werner, M., and Lohmann, G.: Water isotopes – climate relationships for the
877 mid-Holocene and preindustrial period simulated with an isotope-enabled version of MPI-
878 ESM, *Clim. Past*, **15**, 1913–1937, <https://doi.org/10.5194/cp-15-1913-2019>, 2019.

879 Shi, X., Cauquoin, A., Lohmann, G., Jonkers, L., Wang, Q., Yang, H., Sun, Y., and Werner, M.:
880 Simulated stable water isotopes during the mid-Holocene and pre-industrial periods using

881 AWI-ESM-2.1-wiso, *Geosci. Model Dev.*, **16**, 5153–5178, <https://doi.org/10.5194/gmd-16-5153-2023>, 2023.

883 References

884 Gelman, A., Hwang, J. and Vehtari, A.: Understanding predictive information criteria for
885 Bayesian models. *Stat. Comput.*, Springer US, 24, 997-1016, 2014.

886 Gierz, P., Werner, M., & Lohmann, G. (2017). Simulating climate and stable water isotopes
887 during the Last Interglacial using a coupled climate-isotope model. *Journal of Advances in
888 Modeling Earth Systems*, 9(5), 2027-2045.

889

890 Malevich, S. B., Vetter, L., and Tierney, J. E.: Global core top calibration of $\delta^{18}\text{O}$ in planktic
891 foraminifera to sea surface temperature, *Paleoceanogr. Paleoclimatol.*, 34, 1292–1315,
892 2019.

893 Peyron, O., & Vernal, A. D. (2001). Application of artificial neural networks (ANN) to high-
894 latitude dinocyst assemblages for the reconstruction of past sea-surface conditions in Arctic
895 and sub-Arctic seas. *Journal of Quaternary Science: Published for the Quaternary Research
896 Association*, 16(7), 699-709.

897

898

899

900

901

902

903

904

905

906

907

908

909

910

911

912

913

914 **Response to reviewer 3**

915 This is a review comment on the manuscript by Caley et al submitted to Climate of The Past.

916 In this paper, the authors present a calibration effort of sea surface water density and $\delta^{18}\text{O}$
917 analyzed in mixed layer dwelling planktonic foraminifers from core top samples. This is a
918 laudable effort as sea water density is a key parameter driving and responding to
919 oceanographic changes. Agreeing with the comments made by the other reviewer, I will
920 focus on some caveats of the calibration effort. These caveats limit the applicability of the
921 calibration equation in extreme climates of the past. Hence, this limitation needs to be clearly
922 spelled out.

923

924 • It stands out that in the high salinity regions (Med Sea, Arabian Sea, Red Sea,
925 upwelling region off NW Africa) the estimated density is less sensitive to an increase
926 in $\delta^{18}\text{O}_{\text{C}}$. This is clearly visible in Fig 1 (poly1_hier) when an increase of $\delta^{18}\text{O}$ by 3
927 per mill is not accompanied by a substantial predicted density change. This is an issue that
928 is further highlighted in Figure 3 (lower panel), where the residual density (predicted
929 minus observed) shows a strong correlation with salinity changes. This means that
930 the salinity role in shaping the predicted density is underestimated.

931 Though less severe, this issue is also observed in low salinity regions such as the Gulf of
932 Guinea (eastern equatorial Atlantic) and the Bay of Bengal (Northern Indian Ocean).

933 The implication of these observations/caveats is that the current density- $\delta^{18}\text{O}$ calibration
934 (as presented in this paper) is less reliable for the density reconstruction of past extreme
935 climates. For instance, high $\delta^{18}\text{O}_{\text{C}}$ values driven large ice volume, dry climate or ocean basin
936 characterized by anti-estuarine circulation, like the current Mediterranean Sea and Red Sea).
937 Similarly, in warming climate and wet climate (small ice sheet and large riverine runoff), this
938 calibration is likely to provide density estimates with a large uncertainty.

939 While the calibration effort presents a step forward, the authors need to clearly emphasize
940 the serious issues spelled out above. Consequently, the concluding statement made in lines
941 465-475 is too optimistic and needs some moderation.

942 We highlight the high salinity regions mentioned by reviewer 3 in the $\delta^{18}\text{O}_{\text{C}}$ -density
943 calibration on Figure a (with regions = Med Sea, Arabian Sea, Red Sea, upwelling off NW
944 Africa).

945

946

947

948

949

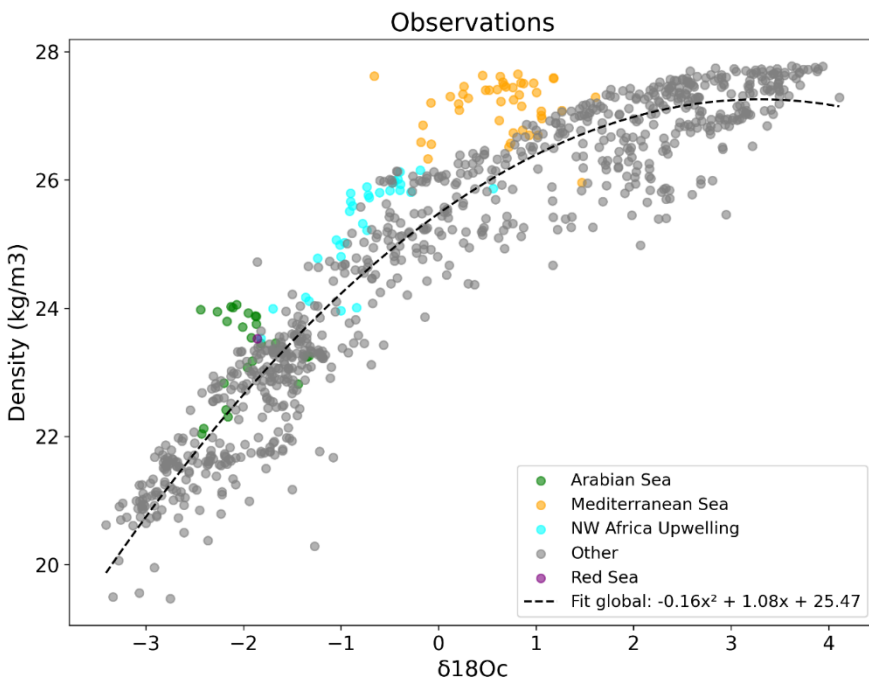


Figure a: $\delta^{18}\text{Oc}$ -density relation for late Holocene core-top samples against observed density. We highlight in colors the high salinity regions mentioned by reviewer 3 (Med Sea, Arabian Sea, Red Sea, upwelling region off NW Africa).

Contrary to what is stated by the reviewer 3, these regions do not correspond to the portion of our calibration curve that is less sensitive to an increase in $\delta^{18}\text{Oc}$ (“**increase of d18O by 3 per mill is not accompanied by a substantial predicted density change**”). In fact, except for some parts of the Mediterranean Sea, these regions are not regions where we observe the maximum ocean density.

In addition, we do not consider that Figure 3 shows a “**strong**” correlation between the residual density and salinity changes. $R^2 = 0.2$ is a weak correlation. Also, this pooled foraminifera species correlation integrates various species. The correlation coefficients with SSS vary for the individual species: $R^2 = 0.17$ for *G. ruber*, $R^2 = 0.12$ for *T. sacculifer*, $R^2 = 0.54$ for *G. bulloides*, $R^2 = 0.15$ for *N. incompta*, and $R^2 = 0.32$ for *N. pachyderma* as discussed in the text. So, probably other factors than SST and SSS influence these residual structures that persist and some of them could indirectly be associated with gradients in SSS. For example, negative residuals are observed in the Benguela, Canary, Peru and North Arabian regions (Fig. 1). All these coastal areas correspond to upwelling systems and previous work already suggested that foraminifera species could have a preference for nutrient-rich waters with high turbidity. This is particularly true for the seasonal species *G. bulloides* (Peeters et al., 2002; Gibson et al., 2016). The negative density residuals in these upwelling regions may reflect this habitat preference (Fig. 1), as we discussed in the text.

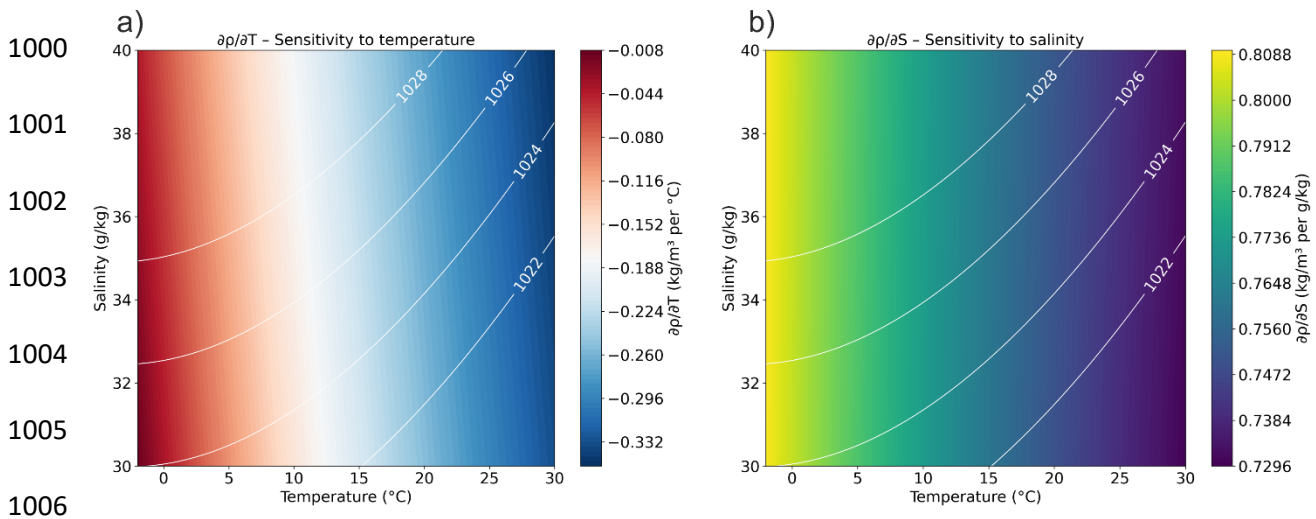
985

986

987 The portions of the calibration curve that can be described by “when an increase of $\delta^{18}\text{O}$ by
 988 3 per mill is not accompanied by a substantial predicted density change” correspond to some
 989 high latitude regions (Nordic Seas and Austral Ocean), as also discussed in the response to
 990 reviewer 2. This is because we are close to the maximum of density observed today.

991 What is the explanation of this decrease in linearity of the relation between $\delta^{18}\text{Oc}$ and
 992 surface ocean density in Nordic Seas and Austral Ocean regions? When density is already
 993 high, **temperature changes have a smaller effect**. Cold water is already dense, so cooling it
 994 further doesn’t increase density as much (see TS diagram on Figure b). Consequently, we
 995 observe a **sensitivity decreases**. The rate of change of density with respect to T flattens out,
 996 meaning the system becomes less responsive to temperature changes. Small changes in
 997 temperature and salinity no longer cause significant shifts in density. This behavior is linked
 998 to the non-linearity of the seawater equation of state.

999



1000

1001 Figure b: TS diagram for Surface Ocean with the derivative $\partial\rho/\partial T$ in (a) and $\partial\rho/\partial S$ in (b). The
 1002 derivative $\partial\rho/\partial T$ and $\partial\rho/\partial S$ represents the change in density per degree of temperature or
 1003 per one salinity unit respectively. In surface waters, and at low temperatures (e.g., -2 to
 1004 2 °C), water is already dense and a temperature change has little effect: $\partial\rho/\partial T$ approaches
 1005 zero. $\partial\rho/\partial S$ remains positive and relatively stable, often between 0.6 and 0.8 kg/m³ per g/kg,
 1006 though it may increase slightly with salinity. Its effect becomes dominant in cold waters,
 1007 where $\partial\rho/\partial T$ is weak. Both diagrams include isopycnals (lines of constant density) and have
 1008 been computed with the Gibbs SeaWater (GSW) Oceanographic Toolbox of TEOS-10.

1009

1010 This process does not affect the $\delta^{18}\text{Oc}$ (quasi-linear fractionation with temperature at low
 1011 temperature (see for example Mulitza et al., 2003)) and this is why we observe that an
 1012 increase of $\delta^{18}\text{Oc}$ by 3 per mill is not accompanied by a substantial change in predicted
 1013 density in Nordic Seas and Austral Ocean. Even if this part of the regression is less predictive,
 1014

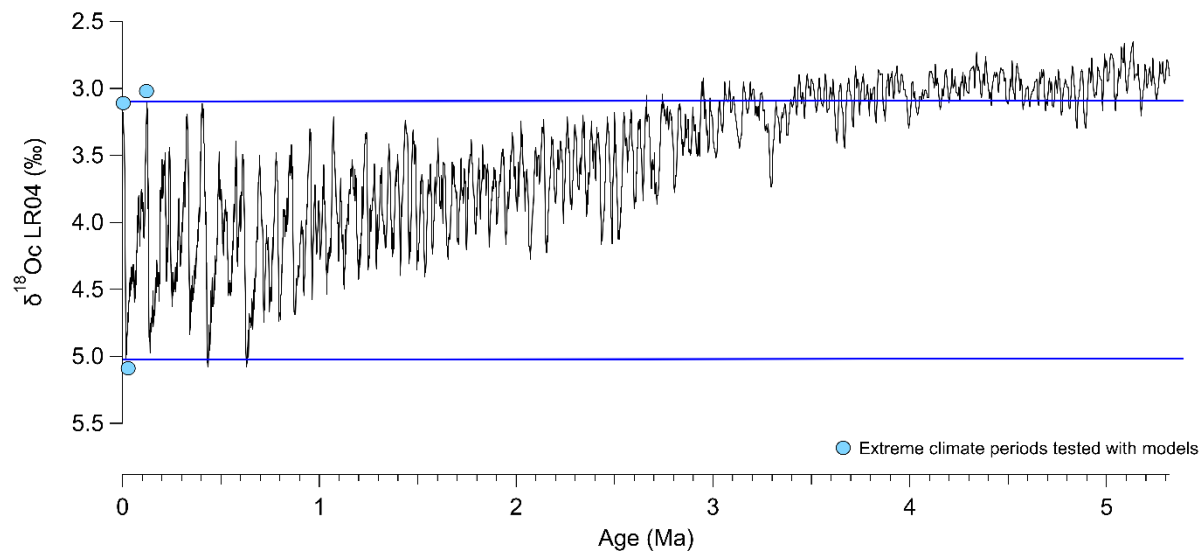
1019 the estimated values of density are correct and are not expected to change strongly as ocean
1020 surface density approaches its upper limits.

1021 In the climate model world, we found some uncertainties, in the Nordic seas, in the model
1022 simulations we conducted at the LGM because of the difficulty to simulate this region (see
1023 response to reviewer 2), together with ocean dynamic effect induced by the mean ocean
1024 salinity increase due to ice volume increase in regions of sea ice and deep water formation
1025 (see response to point 1 of reviewer 1). We therefore recommend in our paper to not apply
1026 the calibration to this region.

1027 Regarding the fact that the calibration could be less reliable for the density reconstruction of
1028 past extreme climates. Concerning “**high $\delta^{18}\text{O}_{\text{C}}$ values driven large ice volume**”, a global
1029 correction can be applied to account for the effect of ice volume increase on $\delta^{18}\text{O}_{\text{sw}}$ and
1030 salinity, and in turn on density (see our response to reviewer 1’s point 1 for detailed
1031 explanations). Because it is an additional global correction, it will not change the range of
1032 values in our present day calibration.

1033 Concerning changes between “**dry and wet climates (small ice sheet and large riverine
1034 runoff)**”, we conducted additional test with model simulations to investigate if the
1035 calibration is likely to provide density estimates with a larger uncertainty. We agree that it is
1036 interesting to put into context our results regarding other climate periods. As asked by the
1037 reviewer 1 in point 9, we conducted some preliminary tests using isotope-enabled model
1038 runs of the mid-Holocene (e.g., Shi et al. 2023). According to reviewer 1, the strongest
1039 precipitation changes (and hence changes in surface $\delta^{18}\text{O}$ and salinity) occur in the early to
1040 mid-Holocene with the strengthening of the Monsoon. Our results clearly indicate a strong
1041 stability of foraminifera $\delta^{18}\text{O}_{\text{C}}$ -density relation between the mid-Holocene (MH) and pre-
1042 industrial (PI) and thus a very weak influence of $\delta^{18}\text{O}$ /Salinity relation instability on final
1043 density predictions. Therefore uncertainties remain within the 95% confidence interval of
1044 our calibration (see our response to point 9 of the reviewer 1). We also conducted additional
1045 tests for the last interglacial period (LIG) as requested by reviewer 2 and found a similar
1046 conclusion (see our response to reviewer 2 point “**I would like the authors to put into
1047 context their results regarding other climate periods**” for results). We already tested in the
1048 initial version of our paper the extreme cold and arid climate of the LGM and found that
1049 additional uncertainties are small and that our approach is valid (except for the Nordic Seas
1050 region), within propagated uncertainties from calibration into predictions of past climate
1051 conditions.

1052 So, even if the salinity role in shaping the predicted density could be slightly underestimated
1053 (indirectly because of foraminifera ecology) for the present day calibration, applying our
1054 calibration to past extreme climates (and taking into account ecological changes) provide
1055 density predictions within the uncertainties of the calibration as demonstrated for the LGM,
1056 and now also for the MH and LIG time periods. Note that these time periods correspond to
1057 extreme climate configurations over the quaternary period as visible on Figure c, so it is
1058 reasonable to state that the new calibration has great potential to be applied to other past
1059 periods and to reconstruct the past temporal evolution of ocean surface density over the
1060 Quaternary (last 2.6 Ma).



1061

1062 Figure c: $\delta^{18}\text{O}$ benthic foraminifera curve (LR04, Lisiecki and Raymo, 2005). Benthic $\delta^{18}\text{O}$
 1063 reflects ice volume and deep ocean temperature changes and is used here to highlight
 1064 extreme climatic periods (colder and more arid glacial periods versus warmer and more
 1065 humid interglacial periods). Extreme climate periods tested with isotope-enabled model runs
 1066 representing the mid-Holocene, LIG and LGM are represented by blue dots. Blue lines
 1067 indicate the range of extreme climate conditions investigated with our climate simulations
 1068 tests.

1069

1070 Nonetheless, we agree with reviewer 3 that under very extreme climates outside the
 1071 quaternary (see Figure c) and in ocean basin characterized by anti-estuary circulation, like
 1072 the current Mediterranean Sea and Red Sea, our calibration could provide density estimates
 1073 with larger uncertainty, a point that requires further investigations.

1074 The additional tests we conducted during the review process for the MH and LIG time
 1075 periods allow us to put our results regarding other climate periods into context. We
 1076 therefore included these results in the new Appendix B. “Application of our calibration to
 1077 other past periods” in the revised version, together with an explanatory text to support and
 1078 reinforce our conclusion about the new calibration and its application to other past periods.

1079

1080 In the revised version we moderate the concluding statement made in lines 465-475 by
 1081 adding in the abstract: “The new calibration has great potential to reconstruct the past
 1082 temporal evolution of ocean surface density over the Quaternary. Under climates outside
 1083 the Quaternary period and in ocean basins characterized by anti-estuary circulation, like the
 1084 current Mediterranean Sea and Red Sea, our calibration could provide density estimates
 1085 with larger uncertainty, a point that requires further investigations.”

1086 And we revised the conclusion as follows: "We demonstrate that our approach is valid to
1087 quantitatively reconstruct annual surface density during one of the coldest climates of the
1088 Quaternary period. We also demonstrate this for the mid Holocene and last interglacial
1089 periods (Appendix B). Hence, our calibration has great potential to be applied to other past
1090 periods and to reconstruct past temporal evolution of ocean surface density downcore
1091 during the Quaternary. Under very extreme climates outside the Quaternary (Appendix B)
1092 and in ocean basins characterized by anti-estuary circulation, like the current Mediterranean
1093 Sea and Red Sea, our calibration could provide density estimates with larger uncertainty, a
1094 point that requires further investigations."

1095

1096 References

1097 Lisiecki, L. E., & Raymo, M. E. (2005). A Pliocene-Pleistocene stack of 57 globally distributed
1098 benthic $\delta^{18}\text{O}$ records. *Paleoceanography*, 20(1).

1099

1100 Mulitza, S., Boltovskoy, D., Donner, B., Meggers, H., Paul, A., & Wefer, G. (2003).
1101 Temperature: $\delta^{18}\text{O}$ relationships of planktonic foraminifera collected from surface waters.
1102 *Palaeogeography, Palaeoclimatology, Palaeoecology*, 202(1-2), 143-152.

1103